Biogeochemical cycling of zinc and its isotopes in the Southern Ocean

Author(s):
Zhao, Ye; Vance, Derek; Abouchami, Wafa; De Baar, Hein J.W.

Publication date:
2014-01-15

Permanent link:
https://doi.org/10.3929/ethz-b-000071944

Originally published in:
Geochimica et Cosmochimica Acta 125, https://doi.org/10.1016/j.gca.2013.07.045

Biogeochemical cycling of zinc and its isotopes in the Southern Ocean

Y. Zhao[1], D. Vance[1,2,*], W. Abouchami[3,4], H.J.W. de Baar[5]

[1] Bristol Isotope Group, School of Earth Sciences, University of Bristol, Wills Memorial Building, Bristol, BS8 1RJ, UK.

[2] Institute of Geochemistry and Petrology, Department of Earth Sciences, ETH Zürich, NW D81.4, Clausiusstrasse 25, Zürich 8092, Switzerland.

[3] Max Planck Institute for Chemistry, P. O. Box 3060, 55020 Mainz, Germany.

[4] Institut für Mineralogie, WWU Münster, Corrensstraβe 24, Münster, Germany.

[5] Royal Netherlands Institute for Sea Research, P.O. Box 59, 1790 AB Den Burg, The Netherlands.

*Corresponding author, tel: + 41 44 632 6881; fax: +41 44 632 1376; e-mail: derek.vance@erdw.ethz.ch.

11 figures.
3 tables
Electronic Supplementary Material

Keywords: GEOTRACES, Southern Ocean, biogeochemistry, zinc, isotopes

ABSTRACT

We report Zn concentration and isotope data for seawater samples from the Atlantic sector of the Southern Ocean, collected during the IPY/GEOTRACES ANT-XXIV/III cruise along the Greenwich Zero Meridian. Data are reported for the full depth range of the water column at three stations, as well as a transect of surface samples, using a new analytical approach that is presented in detail here.

Zn concentrations increase with depth, though due to proximity to upwelling sites, surface concentrations are not as low as in some parts of the ocean such as further northward into the sub-Antarctic zone. For two depth profiles south of the Polar Front Zone, the physical stratification of the upper water column is reflected in sudden near-surface changes in Zn concentration with depth. In contrast, beneath 100-300m Zn concentrations barely change with depth. Zn isotopic data beneath 1000m, for the Southern Ocean data presented here as well as published data from the North Atlantic and North Pacific, are strikingly homogeneous, with an average δ^{66}Zn = +0.53±0.14‰ (2SD, 2SE = 0.03, n = 21). The surface Southern Ocean is more variable, with δ^{66}Zn ranging from 0.07-0.80‰. Between the two is a thin horizon at 40-80m which, in the Southern Ocean as well as the North Atlantic and North Pacific, is characterized by distinctly light isotopic signatures, with δ^{66}Zn about 0.3‰ lower than surface waters.

Strong correlations between Si and Zn concentrations seen here and elsewhere, coupled to the lack of any systematic relationship between Si and Zn isotopes in the Southern Ocean, suggest that the removal of Zn associated with diatom opal involves little or no isotopic fractionation. Regeneration of this Zn also explains the homogeneous Zn isotopic composition of the global deep ocean so far sampled. However, the low Zn content of opal requires that deep ocean Zn does not directly come from the opal phase itself, but rather from associated

organic material external to the diatom frustule during growth. Experimental data are consistent with little or no fractionation during incorporation of Zn into this material. On the other hand, the light zinc at 40-80m is most consistent with the regeneration of an intra-cellular pool that both culturing experiments and field data suggest will be isotopically light. The data thus imply two processes by which Zn is taken up in the surface ocean, that these pools have very different regeneration lengthscales, and that physical mixing of the oceans cannot eradicate their isotopic signatures. Finally, the deep δ^{66}Zn ocean value is significantly higher than the current best estimate of the input to the oceans. The most obvious candidate for the required light sink is the survival of some of the cellular Zn to be buried in sediment.

1. INTRODUCTION

Zinc (Zn) is involved in a number of biological processes in marine micro-organisms (see recent review by Sinoir et al., 2012), such as the important role as a cofactor in the enzyme carbonic anhydrase (Lippard and Berg, 1994) that promotes CO_2 uptake in marine algae (Morel et al., 1994). Moreover, Zn displays nutrient-like depth profiles in the oceans (Bruland, 1980; Martin et al., 1989). For example, in the open Pacific, surface water concentrations of Zn are up to a factor of 250 times lower than those of deep waters, reflecting intense removal of Zn into phytoplankton at the surface and regeneration at depth (e.g. Lohan et al., 2002). In the surface ocean ~98% of total dissolved Zn is chelated with strong Zn-binding organic ligands (Bruland, 1989; Donat and Bruland, 1990; Ellwood and van den Berg, 2000; Lohan et al., 2002; Bruland and Lohan, 2003), so that the concentration of bio-available Zn^{2+} (Sunda and Huntsman, 1992) is typically only 2 – 14 pM in the photic zone of the open Pacific Ocean (Donat and Bruland, 1990). It has been suggested based on laboratory studies that, at this level, Zn could limit phytoplankton growth (Brand et al., 1983; Buitenhuis et al., 2003; Shaked et al., 2006; Sunda and Huntsman, 1992; Sunda and Huntsman, 1995; Sunda and Huntsman, 2005), though other evidence for such limitation is equivocal (e.g. Crawford et al., 2003; see recent review by Sinoir et al., 2012).

It is well known that photosynthetic uptake of carbon and the major nutrients (e.g. Altabet and Francois, 1994; Kroopnick, 1985; De La Rocha et al., 1998) involves a kinetic isotope fractionation such that, for example, phytoplankton preferentially take up ^{12}C over ^{13}C, leading to enrichment in ^{13}C in surface waters. If the depletion of Zn in ocean waters is associated with a similar isotopic fractionation, then Zn isotopes could potentially be used to probe the mechanisms for Zn uptake and export from the surface ocean and, moreover, be used as a paleoceaonographic tracer in similar ways to foraminiferal $\delta^{13}C$ (e.g. Andersen et al., 2011). Precise isotopic analysis of Zn (Maréchal et al., 1999) has only become possible

since the development of multiple collector inductively coupled plasma mass spectrometry (MC-ICPMS). Significant isotopic fractionation of Zn in marine and environmental systems (roughly 2.5‰ total variation in δ^{66}Zn, see data compiled in Cloquet et al., 2006), resulting from equilibrium and kinetic reactions during both biological and abiotic processes, have since then been found in a number of studies, highlighting the potential of Zn stable isotopes as tracers (e.g. Maréchal et al., 1999, 2000; Weiss et al., 2005; Bermin et al., 2006).

In this paper we present, for the first time, depth profiles of Zn concentrations and isotopic compositions covering the entire water column, specifically from the Atlantic Sector of the Southern Ocean. The Southern Ocean is a key region for many global oceanic processes (Marinov et al., 2006), with water from all three oceans coalescing and mixing at depth. It is also an extensive High Nutrient–Low Chlorophyll (HNLC) region (Minas et al., 1986), where trace metals (e.g. Fe) are often cited as the limiting factor for primary productivity (e.g. Boyd and Ellwood, 2010). The aim of this contribution is therefore to assess the extent to which Zn isotope data can clarify the cycling of Zn in a region of the ocean where trace metals are biogeochemically important.

2. OCEANOGRAPHIC SETTING

The study region, at or near the Greenwich or Zero Meridian (Fig. 1), encompasses the eastward flowing Antarctic Circumpolar Current (ACC), which extends to its southern boundary (SB-ACC) from the Sub-Tropical Front (STF), and the Weddell Gyre, which extends from the SB-ACC to near the Antarctic continent. Within the ACC there are two more distinct fronts, the Sub-Antarctic Front (SAF) and the Antarctic Polar Front (APF). Within these latter frontal zones, which are narrow at any one time but meander through time, the ACC flows eastwards about 3-4 times more rapidly than outside them (Orsi et al. 1995).

115 The positions of the fronts during the cruise is shown in Fig. 1. Between the fronts are three
116 wide zones of slower eastward flow (Orsi et al. 1995), the Sub-Antarctic Zone (SAZ) between
117 the STF and SAF, the Polar Frontal Zone (PFZ) between the SAF and APF, and the Antarctic
118 Zone between the APF and SB-ACC. The Weddell Gyre comprises an eastward branch in the
119 ~58 to 65°S region, and a westward return flow in the ~65 to 69°S region, the latter separated
120 from the Antarctic continent by the narrow, eastward flowing, Antarctic Coastal Current.

121 The Southern Ocean comprises all waters south of the STF. The APF is a boundary that is
122 very significant for this study, as follows. Briefly the hydrography of the Southern Ocean is
123 dominated by upwelling along the important frontal regions (Orsi et al., 1995, Fig. 1).
124 Upwelling of Circumpolar Deep Water (CDW) brings waters rich in major nutrients (nitrate,
125 phosphate and silicate) to the surface (Fig. 2). Part of these waters flows northwards where at
126 the APF two processes take place. Firstly some portion of the northward flowing water is
127 subducted at and beyond the APF to become Antarctic Intermediate Water (AAIW), relatively
128 rich in N, P and Si, flowing northwards at typically ~1000m depths far into the Atlantic,
129 Pacific and Indian Ocean basins. Another portion of the northward-flowing water remains at
130 the surface so that, at the APF, very intense summer blooms of large size classes of highly
131 silicified diatoms (Si/N_{diatom} >3) utilize all available silicate (Queguiner et al., 1997). As a
132 result, north of the APF, dissolved silicate is depleted in surface waters, while nitrate and
133 phosphate decrease more gradually until final depletion at the Sub-Antarctic Front (SAF).
134 Another portion of the upwelled nutrient-rich waters flows southwards where eventually, due
135 to intense winter cooling and sea-ice formation in austral winter in the Weddell Sea, the water
136 sinks to form Weddell Sea Bottom Water (WSBW), which eventually flows northward as
137 nutrient-rich (N, P and Si) Antarctic Bottom Water (AABW).

138 The general summer depletion of all three major nutrients in surface waters north of the SAF
139 implies that the northernmost Sub-Antarctic Zone (the SAZ, between the SAF and STF) of
140 the Southern Ocean can actually become macronutrient-depleted. In other words traveling
141 from north to south the surface waters of the Southern Ocean have three distinct regimes of
142 major nutrients: (i) the SAZ that in summer can become depleted in all three major nutrients
143 N, P and Si; (ii) the PFZ that is HNLC for two major nutrients N and P, but depleted in Si;
144 (iii) the Antarctic Ocean south of the APF, comprising the AAZ and Weddell Gyre, that is
145 truly HNLC. In other words, the SAZ is in fact non-HNLC and limiting for all phytoplankton
146 species, the PFZ is Si-limited for diatoms but has ample N and P for other phytoplankton
147 species, and only the Antarctic Ocean is fully HNLC for all three major nutrients i.e. there is
148 an adequate supply for growth of diatoms and all other phytoplankton such that, here, other
149 limitation(s) must exist. These distinctions are important here because in the other major
150 oceans the vertical distribution of dissolved Zn has been shown to correlate strongly with
151 dissolved silicate (e.g. Bruland, 1980). Therefore in this study of Zn and its isotopic
152 composition, the APF is the distinct boundary between true HNLC conditions south of the
153 APF, as opposed to Si-limitation north of the APF. Accordingly, in terms of the major
154 nutrients and potential relationships with Zn and its isotopes, we focus here on Si rather than
155 N and P.

156 Possible limiting factors for productivity in the HNLC zone include iron (Martin et al., 1990;
157 de Baar et al., 1990; Buma et al., 1991; de Baar et al., 1995), light (Mitchell et al., 1991;
158 Sunda and Huntsman, 1997; de Baar et al., 2005), and zooplankton grazing (Cullen, 1991).
159 Initial Fe fertilization experiments generally showed a much stronger response than those with
160 addition of other bio-essential trace metals, such as Mn, Co, Cu, Zn, or combinations thereof
161 (Buma et al., 1991; Scharek et al., 1997). Since then most studies of the role of trace metals in
162 the Southern Ocean (Boyd et al., 2000) have focused on iron (see recent review in Boyd and

163 Ellwood 2010). More recently the covariance of dissolved Mn and phosphate in upper waters
164 of the same Greenwich meridian suggests some co-limitation of Mn and Fe at some times and
165 places in the Antarctic Ocean (Middag et al., 2011a). Also it has been suggested that sub-
166 optimal Zn concentrations in the Southern Ocean may influence Si and N uptake rates by
167 phytoplankton (Hassler et al., 2012). Previous water column work (Coale et al., 2005) has
168 revealed that Zn concentrations, like the major nutrients, are high near the upwelling zone in
169 the Antarctic Ocean and decline sharply northwards.

170 Andersen et al. (2011) have measured Southern Ocean core-top diatom$_{opal}$ samples extracted
171 from marine sediments and reported systematic changes in δ^{66}Zn associated with surface
172 water Zn concentrations. These systematic changes were found to be coupled to changes in
173 Zn/Si ratios of the diatom$_{opal}$, which had been suggested previously (e.g. Ellwood and Hunter,
174 2000; Andersen et al., 2011) to reflect the concentrations of bio-available Zn in the ambient
175 surface seawater where the diatom$_{opal}$ was formed. The δ^{66}Zn and Zn/Si of diatom opal,
176 therefore, have the potential to be used for investigating Zn cycling and primary productivity
177 in the past Southern Ocean.

178

179 ## 3. SAMPLES

180 The seawater samples used in this study, were collected during cruise ANT-XXIV/3 (Feb-
181 April 2008) in the Atlantic sector of the Southern Ocean as part of the International
182 GEOTRACES program and a contribution to the International Polar Year (IPY). Seven
183 vertical profiles were taken, of which 3 were available for study here (Fig. 1, 2). These are at
184 station 104 in the Si-depleted PFZ of the ACC, station 113 in the Si-N-P-rich HNLC AAZ
185 region of the ACC, and station 163 in the Si-N-P-rich HNLC southernmost westward flowing
186 branch of the Weddell Gyre. In addition, large (20 litres) surface water samples (2-5m) were

obtained along the Greenwich Zero Meridian from 47°S to 68°S (Fig. 1), some of which were also available for study here. These are at station 105 in Si-depleted waters of the PFZ, stations 109, 111, 114, 117, 120 in the Si-N-P-rich HNLC AAZ region of the ACC, and stations 123, 126, 129, 133, 136, 139 in the Si-N-P-rich HNLC of the northernmost eastward flowing branch of the Weddell Gyre. Unfortunately, the surface samples that are likely to be the most Zn-depleted, around and northward of the Sub-Antarctic Front, were exhausted by other analyses and not available to us for study.

The TITAN trace metal clean rosette system from the Royal Netherlands Institute for Sea Research (NIOZ) was used for seawater sampling (de Baar et al., 2008). The system consisted of a titanium frame fitted with a standard Seabird CTD in a titanium housing, and 24 modified 12 litre Teflon coated GO-FLO bottles deployed with a kevlar wire with internal signal cables (de Baar et al., 2008). Sample bottles were tripped on the upcast using standard Seabird CTD software. Upon recovery, the complete rosette was carefully moved into its dedicated NIOZ Class-100 clean room container specially built for sub-sampling, where filtration and sub-sampling were performed on the seawater samples using established protocols (Middag et al., 2011b). All seawater samples collected were acidified for storage to pH of around 2 using Seastar HCl. Bottles for sample collection were pre-cleaned with hot acid in the clean labs at MPI. High density polyethylene (HDPE) containers of variable sizes for samples from different water depths (20 litre for surface, 10 litre for intermediate, 5 litre and 1 litre for deep) were subjected to a hot cleaning procedure consisting of successive treatment in alkaline detergent and 6 M HCl, followed by several ultra-pure MQ water rinses to remove trace metal impurities. Sub-sampling for Zn isotopic analysis was done in the clean lab of MPI. Bottles for sub-sampling were supplied by Bristol and pre-cleaned in 20% HCl for 2 weeks, then rinsed 4 times with MQ before packing.

Major nutrients were analyzed onboard by NIOZ using a Bran & Luebbe Traacs 800 Auto-analyser by standard methods described in Grasshoff et al. (1999). Samples for nutrient measurement were obtained from a CTD rosette sampler (an ultraclean CTD) in a polyethylene vial, stored in the dark at 4°C and analyzed within 12 hours of sampling (Fahrbach & de Baar, 2010). A vertical section of measured silicate is plotted along the Greenwich Zero Meridian in Fig. 2. As discussed above, the low Si concentration in SAZ and PFZ in Fig. 2 is the result of the northward transport of upwelled Si-rich CDW water (south of 49°S), with the strong removal of silicate at the APF.

4. METHODS

In order to extract Zn, present at nanomolar (nM) levels or lower, from up to several litres of seawater, an initial pre-concentration is required before purification for isotopic analysis. Preliminary data from this laboratory (Bermin et al., 2006) used both Chelex-100 (Kingston et al., 1978) and co-precipitation with $Mg(OH)_2$ (Wu and Boyle, 1998). Extraction with Chelex-100 is adequate for high Zn concentration deep ocean samples, but for Zn-poor surface samples the blank contribution from the Chelex column is unacceptably high (Bermin et al., 2006). Co-precipitation with Mg is achieved by adding ammonia to acidifed samples until the seawater's own inventory of dissolved Mg precipitates at pH~10 as $Mg(OH)_2$, bringing virtually all of the Zn with it. Again, this procedure performs adequately for Zn-rich deep ocean samples where relatively small volumes (<500 mL) of seawater can be used. However, for the large samples required to obtain enough Zn from depleted surface samples (in some case >2 litres in this study), the Mg precipitate is so large that it causes difficulties during the subsequent separation and purification of Zn.

Here, a new pre-concentration approach has been used, involving the addition of a Zn-free

aluminium solution to the seawater sample. The pH is then raised with ammonia, but in this case only to about 8.5-9.0 so that $Al(OH)_3$ precipitate is produced but no $Mg(OH)_2$. Since the amount of aluminium added can be controlled, subsequent handling of the precipitate during the chromatographic purification of Zn is much easier. Since these are the first data we report using this approach, we describe it in some detail in this section, including the tests we have undertaken to establish its success. We also take the opportunity to compare the Zn concentrations obtained here with those published previously for the same or similar locations (Löscher, 1999; Croot et al., 2011).

All lab work was carried out under clean laboratory conditions in Class-100 laminar flow clean hoods, using only Savillex (Minnetonka, MN, USA) PFA labware. All labware was cleaned on the hotplate, firstly with 6 M HCl, subsequently with 50% HNO_3 for two days, then with 1% once distilled HNO_3 for another day, rinsing thoroughly between each step and at the end. 18.2 MΩ MQ water was obtained from a Millipore Q-Gard® B1 system. All acids used were distilled twice.

4.1 Pre-concentration by co-precipitation

The initial step of co-precipitation was either done in large pre-cleaned Teflon beakers (up to 1 litre), or in a clean 4 litre LDPE bottle (for samples > 1 litre). Samples were weighed, and Zn double spike and 1.2 ml 10000 ppm Al standard solution were added. The commercial Al solution was pre-cleaned of Zn on an anion column and subsequently re-dissolved in 1M HCl. The ratio between sample and double spike Zn is ideally 1 (Bermin et al., 2006), but there is a lot of leeway in this (see below). Beakers were left to equilibrate overnight, whereupon an ultra-clean ~11M Romil ammonia solution was added to reach a desired pH. White precipitate began to form and the beakers were left for a few more days for the precipitate to develop. After this, as much supernatant as possible was poured off. Then the precipitate and

remaining water was transferred to a smaller pre-cleaned Teflon beaker to settle again. The precipitate was then separated from the remaining supernatant by centrifugation. The centrifuged precipitate was washed with pH = 10 MQ (MQ to which a small amount of ammonia was added) and centrifuged again. The final "clean" precipitate was dissolved in 2 ml 7 M HCl, dried down, taken up in 1 ml 7 M HCl and dried down twice. The sample was finally dissolved in 1ml (or more, depending on the amount of precipitate obtained) 1 M HCl, before passing through the anion exchange column for further purification.

The aluminium solution, despite being pre-cleaned on a column, was a significant contributor to the total blank. In addition, co-precipitation at too high a pH causes precipitation of un-wanted Mg hydroxide from seawater in addition to aluminium hydroxide. Tests were therefore conducted to ascertain the smallest amount of Al solution that could be used, as well as the minimum pH for co-precipitation, while maintaining high Zn yields. Because of the double spike approach, high Zn yields are not essential for accuracy, but they are desirable to maximize the final analyte signal during mass spectrometry. Based upon the results of these tests (see Electronic Supplementary Material (ESM), Fig. 1), it was decided to add 1.2 ml of Al solution (12 mg) and to raise the pH to 8.5-8.8 during co-precipitation. In both cases this procedure produced yields in excess of 90% (Tables 1-3) for sample sizes ≤ 1 litre, and greater than 70% for sample sizes > 1 litre, where quantitative recovery of the precipitate from 4 litre bottles was difficult.

4.2 Column Chemistry

The column procedure described by Maréchal et al. (1999), modified by Archer and Vance (2004), has been adopted, with some further minor modifications. Primarily, 1 M HCl has been used instead of 7 M HCl to dissolve precipitate and eliminate seawater matrix. There were two reasons for this: 1) 1 M HCl would contribute less blank than 7 M HCl; 2) it was

283 easier to dissolve $Al(OH)_3$ in 1 M HCl than in 7 M HCl. Samples were loaded to the column
284 in 1 ml (or 2 ml, depending on the amount of precipitate to be dissolved) 1 M HCl. Most
285 metals were washed off in 12 ml 1 M HCl before Zn was collected in 4 ml 2% HNO_3. A
286 column calibration was performed with Zn JMC standard and the result suggested that no Zn
287 was eluted until 2% HNO_3 was put through the column. The measured column blank of this
288 procedure was 0.2 ng for Zn.

289 **4.3 Procedural Blanks**

290 Quantifying the blank for a co-precipitation procedure is difficult because in order to re-
291 produce the entire procedure a seawater sample that contains a finite amount of Zn must be
292 used, so that all measured blanks will be maxima. Ultrapure water can be used as the
293 "seawater" sample but, again, the large quantities of this that must be used to simulate the
294 measured seawater sample will contain finite amounts of Zn. Here we quantified the
295 maximum blank by extracting Zn from different volumes of MQ water, adding the same
296 amount of Al solution as for samples to each, as well as an amount of ammonia appropriate
297 for an acidified 1 litre seawater sample (the ammonia blank was insignificant relative to other
298 sources at 7 pg/ml). Duplicate sets of results for these MQ "samples" (Figure 2 in the ESM),
299 suggest a procedural blank for real samples of ~2 ng. A further constraint derives from
300 analyses performed on extremely Zn-depleted surface samples from the Equatorial Atlantic,
301 samples that turned out to contain as little as 0.01 nM Zn, as determined by isotope dilution.
302 For these 4 litre samples this implies a total amount of Zn found of about 2.5 ng.

303 All of the above suggests a blank contribution of 2-3 ng, though better quantification could
304 reveal it to be substantially lower. Sample volumes analysed here ranged from 0.1 – 2.2 L,
305 yielding total amounts of Zn analyzed of 34 – 219 ng. With the above absolute maximum
306 procedural blank of 3 ng, the Zn blank contribution to the smallest sample analyzed was less

than 9%. Previous measurements of the isotopic composition of (larger) blanks in this laboratory gave $\delta^{66}Zn$ = 0.17±0.18‰ (Bermin et al., 2006; $\delta^{66}Zn_{JMC\text{-}Lyons}$ = [($^{66}Zn/^{64}Zn_{sample}/^{66}Zn/^{64}Zn_{JMC\text{-}Lyons}$)-1]x1000, where JMC-Lyons refers to the Johnson Matthey zinc standard JMC batch 3-0749, obtained from the lab of Francis Albarède; Maréchal et al., 1999). All samples measured here were corrected for the contribution of a 3 ng blank with an isotopic composition of +0.2‰, but the size of these corrections is insignificant for all measured isotopic compositions compared to other sources of analytical uncertainty. In other words, if the blank contribution was really close to zero, the data reported in the paper would not change by more than about 0.03‰.

4.4 Mass Spectrometry

Isotopic analysis of Zn was performed on a Thermo Finnigan Neptune MC-ICPMS at Bristol at low mass resolution. Samples were introduced into the mass spectrometer in 2% (v/v) nitric acid via an Aridus desolvating nebuliser system (Cetac, Omaha, NE, USA) and desolvating spray chamber. The spray chamber was held at 105°C and the desolvator at 160°C. Typical Ar sweep gas settings were 4.25 – 4.75 L/min with little day-to-day variation in the sweep gas required to obtain the optimum Zn signal. No N_2 was used as ArN_2 would result in interference on ^{68}Zn. All stable isotopes of Zn, as well as ^{62}Ni, ^{63}Cu, ^{65}Cu were collected simultaneously in static mode using a multiple Faraday collector array. Data collection consisted of 30x4s integrations and each measurement was preceded by a blank measurement (15x4s integrations) of the 2% HNO_3 used to make the analyte solutions and followed by a wash or two in clean 2% HNO_3. The blank signal was subtracted from the sample signal and normally amounted to no more than 0.02% of total analyte 64 ion beam.

All Zn isotopic data are reported relative to the Johnson Matthey Zinc standard JMC 3-0749, obtained from the lab of Francis Albarède (Maréchal et al., 1999). The standard delta per mil

notation is used and is defined as:

$$\delta^{66}Zn = \left[\frac{\left({}^{66}Zn/{}^{64}Zn \right)_{sample}}{\left({}^{66}Zn/{}^{64}Zn \right)_{JMC}} - 1 \right] \times 1000$$

Mass discrimination artefacts, that may be introduced at any stage in the chemical and mass spectrometric procedure, were corrected using the double spike method as detailed in Bermin et al. (2006). All uncertainties cited are 2SE of 30 4 second integrations propagated through the full double spike reduction procedure unless specified. To test the robustness of the double spike approach, JMC standard and double spike were mixed at various ratios and analyzed during every analytical session (see Fig. 3 in ESM for data).

4.5 Tests on real seawater samples

Zn isotopic data for samples from the GEOTRACES IC1 intercalibration project (BATS station, 31°40'N 64°10'W) have already been reported by this laboratory (Boyle et al. 2012). No other Zn data were reported for these samples so that we cannot demonstrate inter-laboratory consistency at this stage. However, the duplicates analysed by us and reported in Boyle et al. (2012) are all consistent with each other. Furthermore, analyses of deep ocean samples by S. John and T. Conway (pers. comm. September 2012) are yielding the same results as we obtain here and in Boyle et al. (2012). There are a number of other laboratories now pursuing Zn isotopic measurement of seawater so that we hope that this situation improves soon. With this in mind Table 1 reports data obtained here for other samples from recent intercalibration efforts.

Though no isotopic data have been reported yet for these samples from other laboratories, the concentrations obtained here are consistent with those measured elsewhere with completely independent approaches. Thus the consensus values for Zn in SAFe D1 and D2 are 7.1±0.6

353 and 7.2±0.5 nmol kg^{-1} while that for the SAFe surface sample is also identical to those
354 obtained here at 0.064±0.019 nmol kg^{-1}
355 (http://es.ucsc.edu/~kbruland/GeotracesSaFe/kwbGeotracesSaFe.html). The Bruland
356 laboratory at Santa Cruz has measured 1.42 nmol kg^{-1} for Zn in the Santa Barbara sample,
357 whereas we obtain 1.35 and 1.37 nmol kg^{-1} for two duplicate aliquots from two different
358 bottles.

359 **4.6 Standard-addition tests**

360 Another test of our procedure involves the addition of standard to seawater samples from
361 which Zn has been removed, to seawater samples with very small natural Zn concentrations,
362 and to MQ water, all followed by pre-concentration, column purification and mass
363 spectrometric analysis. Fig. 3 shows results obtained for addition of variable amounts of JMC
364 standard to seawater samples from which Zn had been removed (supernatant poured off from
365 a previous Al co-precipitation, retained and treated as a new "sample") and MQ. The result
366 for the seawater samples was $\delta^{66}Zn = +0.08 \pm 0.03‰$ (n = 12), and for MQ $\delta^{66}Zn = -0.01 \pm$
367 0.02‰ (n = 8). Although the value for the seawater supernatant samples was close to zero, the
368 data indicate that a small amount of seawater Zn was left in the supernatant after co-
369 precipitation, resulting in the slightly elevated $\delta^{66}Zn$. Evidence for this came from the
370 comparison of seawater supernatant samples with different amounts of JMC standard added.
371 For those with only 30 ng of standard Zn added, the $\delta^{66}Zn$ was more elevated from the
372 expected 0‰ (and also closer to the seawater $\delta^{66}Zn$) than those to which 200 ng of standard
373 Zn was added, due to a larger relative contribution of the residual seawater Zn. A sample
374 calculation illustrates how this is possible. For example, for 30 ng of standard Zn added, the
375 typical shift away from 0‰ at the limits of uncertainty is about 0.1‰ towards the original
376 seawater sample value of +0.46‰. Thus the shift is of the order of 20% of the total difference

377 between the predicted 0‰ and the original seawater sample. This would require an amount of
378 residual seawater Zn of 8 ng. If the yield from the original co-precipitation is 90 – 95%, and
379 given an original amount of Zn in the seawater sample of around 100ng for these samples,
380 then a residual amount of seawater Zn of around 5 – 10 ng is plausible. Data for the MQ
381 samples, which had negligible amounts of Zn originally, all fell within the error of the
382 expected 0‰ (Fig. 3).

383 Another test was performed by adding different amounts of standard JMC Zn to a set of 4 litre
384 samples obtained from the surface Equatorial Atlantic, which through previous analysis by
385 isotope dilution had been found to contain only 0.01-0.03 nmol kg^{-1} sample Zn. The data are
386 illustrated in Figure 4. The good fit of the data to a straight line might be taken to indicate
387 simple mixing between standard Zn ($\delta^{66}Zn = 0$, low 1/Zn) and sample Zn.

388 **4.7 Intercomparison of Zn concentrations with previous data from the Southern Ocean**

389 Seawater samples from locations close to those analysed in this paper have been the subject of
390 two other studies for Zn concentrations (Löscher, 1999; Croot et al., 2011). Direct
391 intercomparison between these studies and ours is made difficult by the fact that the previous
392 studies are not often from precisely the same location, depths etc. Figure 5 shows a depth
393 profile from our Station PS71-113-2 along with data from exactly the same location for
394 samples collected on the same cruise with the same sampling equipment and filtration (Croot
395 et al., 2011), and data from a composite depth profile made up of samples from other nearby
396 sites in the Southern ACC collected in 1992 (Löscher, 1999). The latter dataset is from a time
397 when contamination control during sample collection was a lot more difficult than now, and
398 has some outliers, but it is also clear that the agreement between these data and ours at depths
399 ≥1000m is essentially perfect. The data from Croot et al. (2011), on the other hand, are about
400 25-50% lower than both our data, and the Löscher (1999) data beneath 1000m where a

meaningful comparison can be made. The Croot et al. (2011) data were obtained using simultaneous dithiocarbamate-freon extraction followed by graphite furnace atomic absorption spectroscopy. Since the publication of the Croot et al. (2011) data, it has become apparent that this approach, when performed on samples that have been acidified with HCl, yields Cd concentrations that are up to about 50% lower than by isotope dilution (O. Baars and W. Abouchami, unpublished data). It seems likely that this problem applies also to the Croot et al. (2011) Zn data. It may be related to incomplete stripping of the metals from organic complexes during the pre-concentration step. The problem is particularly apparent in samples that had been acidified with HCl and analysed shortly after acidification, while it can be eliminated for samples that are acidified using oxidizing acids like HNO_3 (P.L. Croot, pers. comm.).

5. RESULTS

5.1 Three vertical profiles along Greenwich Zero Meridian

Data for the three vertical profiles PS71-104-2, PS71-113-2, PS71-163-1 (Fig. 1) analysed in this study for dissolved Zn concentrations and isotopic compositions are presented in Table 2. The data are shown as depth profiles, with other key oceanographic parameters, in Fig. 6-8.

The water column at the most southerly station, **PS71-163-1** (Fig. 6), in the Weddell Gyre, is extremely stratified at the surface, with temperature and salinity increasing quickly from surface minima of -0.8°C and 34, to about 0.9°C and 34.7 at the AASW (Antarctic surface water) - CIW (Central Intermediate Water) boundary at 200m. This stratification must be driven by the low surface salinity, given the sharp 1.7°C decrease in temperature in the surface layer. The AASW-CIW boundary also corresponds to an O_2 minimum. Si is relatively high at the surface (60 μmol/kg) and also increases sharply with depth, but the AASW-CIW

425 boundary is not as sharp as for the physical parameters or O_2. Though there is an inflexion in
426 the Si depth profile at this depth, concentrations continue to increase relatively smoothly
427 through it.

428 The Zn concentration profile looks more like salinity than Si. Zn concentrations are not
429 particularly low at the surface (2.5 nM), and increase quickly to about 7 nM at 74m. Beneath
430 this boundary, salinity, oxygen and Zn are very homogeneous with depth, with Zn
431 concentrations between 7.1 and 7.8 nM. There is a slight maximum (7.8 nM) at 1000 –
432 1500m, close to the CIW-WSDW (Weddell Sea Deep Water) boundary. Si concentrations, by
433 contrast, continue to increase beneath the AASW-CIW boundary and only reach their
434 maximum in the bottom-most sample measured. The δ^{66}Zn profile shows a maximum of
435 +0.67‰ at the surface, in contrast to quite an extreme minimum of +0.27‰ within AASW at
436 45m. Beneath this, from 170 – 4000m, δ^{66}Zn is extremely homogeneous at +0.53±0.10‰
437 (2sd). There is a very slight minimum (+0.44‰ to +0.49‰) at the AASW-CIW boundary,
438 and a very slight, broad, maximum (+0.64‰ at 1000 – 2000m, decreasing to +0.53‰ at
439 4000m), but these features are barely analytically significant. The bottom-most sample shows
440 very anomalous δ^{66}Zn at +0.97‰.

441 Station **PS71-113-2** (Fig. 7) is within the ACC, in the Antarctic Zone to the south of the Polar
442 Front. The major physical oceanographic difference between this station and PS71-163-1 is
443 slightly less extreme stratification, though it is still significant. The upper 100m of the water
444 column has the low salinity that is characteristic of AASW, and is also characterized by
445 homogeneously high dissolved O_2 and moderately low, Si (at 35 μmol kg^{-1}). Potential
446 temperature is more variable at 1.2 – 1.4°C. The core of UCDW (Upper Circumpolar Deep
447 Water) beneath AASW is characterized by a temperature maximum (~1.6°C at 400m) and a
448 slight O_2 minimum (185 μmol kg^{-1} at 400m). Salinity shows a very slight maximum in

449 UCDW. Beneath the core of UCDW, salinity and O_2 remain relatively constant to the bottom.
450 Si in contrast increases sharply at first in UCDW, down to the core of UCDW, and then more
451 slowly but monotonically to the bottom.

452 The pattern of the Zn concentration profile, as with Station PS71-163-1, looks more like
453 salinity and inverse O_2 than Si. AASW at 0 – 100m is characterized by the lowest Zn
454 concentrations, but still relatively high for surface water, at 2.6 – 3.1 nM. There is then a step
455 change into UCDW, resembling the sharp increase in salinity and drop in O_2. UCDW Zn
456 concentrations are homogeneously high at around 6.3 – 6.6 nM. In LCDW (Lower
457 Circumpolar Deep Water), Zn concentrations increase slightly to 6.8 – 7.1 nM, but relative to
458 Si, for example, are relatively homogeneous from 100m to the bottom of the water column.

459 The δ^{66}Zn profile at PS71-113-2 exhibits a clearer structure than that at PS71-163-1. As with
460 PS71-163-1, the δ^{66}Zn profile at PS71-113-2 has a pronounced surface maximum (+0.8‰),
461 and again there is a sharp drop in the sub-surface, to +0.47 to +0.54‰ at 74 – 101m, still
462 within AASW. Note that no sample has been measured at 40-50m in this profile (c.f. more
463 pronounced minima at 40 – 50m at both stations 163-1 and 104-2; Table 2). Uppermost
464 LCDW has a δ^{66}Zn value of +0.70‰ at 1000m. Between AASW and uppermost LCDW,
465 UCDW appears to have a lower δ^{66}Zn, at +0.39‰ to +0.48‰, a minimum that is just about
466 analytically significant relative to the values immediately above and below. Below 1000m,
467 and for the remainder of LCDW down to the bottom at 2351m, the δ^{66}Zn value decreases
468 gradually and monotonically, from the high of +0.70‰ at 1000m to +0.43‰ at the bottom.
469 As noted above, Zn concentrations change very little through this isotopic structure in the
470 lower water column beneath AASW.

471 Station **PS71-104-2** (Fig. 8) is also within the ACC, in the low-Si PFZ, between the APF and
472 the SAF. The upper water column at this station is significantly less stratified than the other

two. This station is in the Polar Frontal Zone formation region of AAIW, and surface salinity is marked by the minimum (33.73) that is characteristic of that water mass. Salinity then increases to a slight maximum (34.78) at 2000m, in the upper levels of NADW (North Atlantic Deep Water, see Fig. 3 of Middag et al., 2011a). The core of UCDW is characterized by the same minimum in dissolved oxygen seen at Station PS71-113-2. Temperature decreases monotonically downward from a surface maximum of 6.5°C, though with inflection points near the boundaries of the main water masses. Surface Si concentrations are much lower than the other two stations – at ~1.9 μM here in contrast to 63 and 35 μM at the other two stations. Si increases monotonically downward, though again with inflection points at the boundaries of the water masses, notably at the UCDW-NADW boundary, above which Si is relatively constant with depth but below which there is a renewed increase.

The Zn concentration profile, in contrast to those at the other two stations studied, looks much more like Si than salinity. Surface Zn concentration is much lower at this station, at 0.32 nM – a feature that mirrors the Si contrast between the three stations. Zn concentrations then increase steeply through AAIW to reach a maximum of ~5.35 nM at 1000 – 1500m in the core of UCDW. This maximum occurs at the same depth as the homogeneous Si concentrations above the UCDW-NADW boundary. Zn concentrations then undergo a renewed increase through NADW and into LCDW, reaching 8.04 nM at 4006m. The bottom-most point has distinctly lower Zn concentration at 7.03 nM.

As with the other two profiles δ^{66}Zn shows a clear change from a higher value right at the surface (+0.47‰) to a minimum at 50m (+0.25‰). Through the remainder of AAIW and UCDW, δ^{66}Zn returns to homogeneously heavier values (at +0.44±0.06‰ at 100 – 2000m), consistent with the values for UCDW seen at Station PS71-113-2 (+0.39‰ to +0.48‰). NADW and LCDW appear to be characterized by slightly heavier values, with two

497 measurements at +0.60‰ and 0.61‰. Again, this is consistent with the heavier values seen in
498 LCDW – up to +0.70‰ – relative to UCDW at Station PS71-113-2. A slightly lower δ^{66}Zn is
499 found in the bottom-most sample than directly above, paired with the distinctly lower Zn
500 concentration in this sample relative to the measurement directly above.

501 **5.2 Surface transect along Greenwich Zero Meridian**

502 In addition to the above depth profiles, samples from 11 surface transect stations PS105,
503 PS109, PS114, PS117, PS120, PS123, PS126, PS129, PS133, PS136, PS139 were also
504 analysed for dissolved Zn concentrations and isotopic compositions. Data are presented in
505 Table 3. The Zn data, with other key oceanographic parameters, are plotted against latitude in
506 Fig. 9.

507 Note that though the Zn concentration reproduces across duplicate analyses of two separate
508 aliquots from the same 20 litre MPI container, the data for Station PS111 (52.17°S) are highly
509 anomalous. We suspect that the original 20 litre MPI bottle must have been contaminated
510 before or during original sampling, and these data are not plotted, nor considered further in
511 the results and discussion sections below. Relatively smooth transitions between the other
512 samples across the latitudinal transect suggest no such problems.

513 The surface transect sampling stations covered, from north to south, the PFZ, the Antarctic
514 Zone (AAZ) of the ACC and the northern end of the Weddell Gyre. The highest Si values are
515 in the Weddell Gyre and the region of strong upwelling in the AAZ of the Southern ACC (c.f.
516 Fig. 2). The peak in surface Zn concentrations also occurs here, but is sharper and centered on
517 58°S, near the boundary between the Weddell Gyre and the Antarctic Circumpolar Current. In
518 fact, as with the depth profiles, the pattern of Zn concentrations in the southern regions of the
519 surface transect most closely matches salinity. Both salinity and Zn have a sharp peak near the
520 boundary between the Weddell Gyre and the Antarctic Circumpolar Current, and more rapidly

declining values north of this as far as about 53°S. Thereafter, further north, the pattern in Zn concentrations begin to look more like that of Si.

δ^{66}Zn is relatively constant at +0.45‰ to +0.6‰ across the Weddell Gyre and into the southern ACC as far as about 53°S (Fig. 9). The only datum that is significantly different along the entire transect is at 48°S (+0.10 ‰).

6. DISCUSSION

6.1 Controls on Zn isotope systematics in surface waters

Overall, the Zn isotope data reported here display a total variation in δ^{66}Zn of about 0.9‰, representing about 40% of the total variation yet reported for Zn isotopes on Earth (see compilation in Cloquet et al., 2006). However, perhaps the most striking aspect of the Southern Ocean depth profiles is their relative homogeneity. Thus, apart from one outlier, the datum for the deepest sample at location PS-71-163-1 (at +0.96‰), the variation in the entire dataset beneath 50m is only at about the 4 sigma level (mean and 2SD = 0.51±0.15‰). There is more variation above 50m, with δ^{66}Zn values as high as +0.8 ‰ and as low as 0.07‰.

Zn depletion in the surface ocean is generally attributed to biological uptake, and enrichments at depth as due to return of Zn to the dissolved pool from particulate material that is biologically-packaged in the photic zone (e.g. Bruland and Lohan, 2003 and Sinoir et al., 2012). If biological uptake of Zn in the surface ocean is associated with even a small isotope fractionation there should be a clear impact on the isotopic composition of the small residual surface pool. Though upwelling of nutrient-rich waters means that surface Zn concentrations are not nearly as low in our study area as in many parts of the ocean (e.g. Bruland, 1980; Lohan et al., 2002; Boyle et al., 2012), it is still the case that Zn concentrations at 5-15m are up to 20 times lower than those of the deep Southern Ocean. Even if the kinetic fractionation

545 associated with cellular uptake of Zn is as small as +0.2‰ ($\delta^{66}Zn_{dissolved} - \delta^{66}Zn_{cell}$), a residual
546 dissolved pool of 5% should be 0.6‰ heavier than the Zn upwelled from the deep ocean,
547 assuming Rayleigh fractionation in a closed system. The implied heavy dissolved phase $\delta^{66}Zn$
548 are not seen in the surface waters analysed here.

549 One obvious potential reason for the lack of an imprint on isotopic compositions of strong
550 apparent vertical Zn cycling is that biological uptake is associated with negligible isotopic
551 fractionation of Zn isotopes. Experimental data that quantifies fractionation of Zn isotopes
552 upon biological uptake are scarce. The single relevant culturing experiment performed thus
553 far (John et al., 2007) suggests that the cellular quota of Zn in an oceanic diatom is 0.2-0.8‰
554 lighter, depending on ambient free Zn^{2+} concentrations that are thought to drive different
555 uptake mechanisms, than the culture medium. This finding is consistent with a single study in
556 a Swiss lake (Peel et al., 2009), where organic-carbon-rich particulates produced during the
557 spring bloom are preferentially enriched in the light isotopes of Zn, by an amount close to the
558 upper end of the isotopic separation implied by the culture experiments.

559 It is also theoretically possible that the intense vertical cycling of Zn in the oceans is
560 dominated by an abiotic process, such as scavenging onto particulate material in surface
561 waters and release back to the dissolved phase in the deep. Such a process has been invoked
562 to explain the vertical distributions of many other trace metals (for example aluminium,
563 thorium, see Bruland and Lohan., 2003 for a review). However, none of these metals show the
564 extreme surface to depth fractionation (up to 200 times lower concentrations in the photic
565 zone than the deep) that Zn does. Moreover, adsorption onto particulate surfaces is also
566 associated with isotopic fractionations that should also lead to deviations in the residual
567 dissolved pool (e.g. Pokrovsky et al., 2005; Gélabert et al., 2006; Balistrieri et al., 2008;
568 Juillot et al., 2008).

569 Perhaps the strongest evidence for the biological cycling of Zn in the oceans is the well-
570 established close correlation between its depth distribution in the oceans and that of silica
571 (Bruland et al., 1980). The generally close association of Si and Zn has led to the suggestion
572 that both are regenerated together through the dissolution of diatom opal in the deep ocean.
573 However, culture experiments have shown that Zn contents of the opal phase of diatom cells
574 are very small, and that 97-99% of the Zn in diatoms is in organic material (Ellwood and
575 Hunter, 2000). Moreover, the Zn/Si ratio of diatom opal is 1-2 orders of magnitude smaller
576 than in the deep Pacific (Bruland, 1980; Ellwood and Hunter, 2000; Lohan et al., 2002), also
577 arguing against the importance of the opal phase as the source of deep ocean Zn. One way to
578 explain the close correspondence of the deep regeneration profiles of Si and Zn, that is also
579 consistent with the lack of Zn in the opal phase, is to invoke a Zn-rich organic phase that is
580 intimately associated with the diatom frustule (c.f. Lohan et al., 2002). Thus, regenerated Zn
581 does not derive from the opal phase itself, but it is only exposed to oxidation in the deep
582 ocean when the opal dissolves. It is well established that polysaccharides and proteins coat the
583 silica frustule of diatoms, and that these bear functional groups (e.g. amino, carboxyl) that
584 have a strong affinity for metal ions, including Zn (e.g. Gélabert et al., 2006).

585 These considerations have two obvious implications for the interpretation of the dissolved
586 phase Zn concentration and isotope data presented here. Firstly, they imply that there is more
587 than one biologically-controlled pathway by which Zn is removed from the surface ocean –
588 into proteins and enzymes within phytoplankton cells in all phytoplankton groups, and into an
589 organic phase that is, physically, intimately associated with the opal frustule of diatoms.
590 These two uptake mechanisms may be associated with different isotopic fractionations and
591 their relative importance will depend on local phytoplankton ecology, thus complicating
592 oceanic Zn isotopic data. Secondly, the regeneration of these two different pools, one at
593 shallower depths in association with intra-cellular organic matter, and one at greater depths

coupled to opal dissolution, could lead to a partial decoupling, both between depth profiles of Zn isotopes and those of Zn (and Si) concentrations, and between the upper and deep ocean.

In the ensuing sections we discuss each of these implications, first for surface data and then for the sub-surface and deep ocean.

6.2 Controls on Zn in surface waters: relationships between Zn isotopes and Si and Zn concentrations

The association between Zn and Si concentrations discussed in the previous section is seen in the Southern Ocean data (Fig. 10a), but there is systematic structure in this relationship. Moreover, Zn isotopes show no relationship at all with either Si (Fig. 10b) or Zn concentrations. We suggest that the structure apparent in the surface water Zn-Si relationship in Fig. 10a, as well as the lack of any coherent relationship with Zn isotopes (Fig. 10b), may both be a consequence of the multiple controls discussed in the previous section. For example, on the Zn-Si plot (Fig. 10a) the upper ocean data (the surface (2-5m) samples with the filled symbols, all profile data from depths above 100m, but down about 300m at 104-2) clearly separate into two arrays with different slopes, corresponding geographically to the Weddell Gyre and the ACC (c,f a similar geographic split for Cd isotope data for these samples; Abouchami et al., 2011). In most of the ACC zone, Zn-Si data for the upper water column follow a tight linear correlation that comes close to going through the origin. In contrast, surface data to the south of about 56°S, within the Weddell Gyre, fall on a much steeper trend. There is a transition zone in the southernmost ACC (53-55°S), where Zn concentrations flatten out at 2.7-2.8 nmol kg^{-1} while Si is variable (Fig. 10a, see also Fig. 9). Data for the deeper levels (all data beneath about 300m) at all stations are at the high concentration end of both trends. Geographically the top ends of both the surface trends, those closest in chemistry to deep waters, are for surface waters in the upwelling zone centered on 58°S.

618 In terms of the ideas discussed in Section 6.1, it is noteworthy that diatoms peak in abundance
619 at 52-56°S, just north of the upwelling zone (Alderkamp et al., 2010). Their proportion of the
620 phytoplankton assemblage then decreases steadily and monotonically northward as the Si
621 supply via horizontal advection from the upwelling zone decreases. The concomitant decrease
622 in Zn along the ACC trend might suggest that Zn concentrations are subject to the same
623 control. In the portion of the Weddell Gyre for which we present surface data, diatoms also
624 decrease in relative importance southwards to be replaced by a peak in haptophytes (60% of
625 total phytoplankton at 62°S; Alderkamp et al., 2010). Though the requirement of haptophytes
626 for Zn is not clear, the lesser importance of diatoms in this region, as well as lower
627 productivity overall, could explain both the high surface Si concentrations in the WG (Fig. 9)
628 and the steep slope of the Zn/Si relationship in Figure 10a.

629 The impact of these changes in microbial ecology are hard to pinpoint at this early stage in the
630 development of oceanic Zn isotopes. But, for example, it may be that the relative lack of
631 correlation between Zn isotopes and Si concentrations (Fig. 10b) is a result of the dominance
632 of Zn removal into an organic phase, such as external polysaccharides that are ultimately
633 associated with the opal frustule, and that does not involve a strong isotopic fractionation.
634 Alternatively, any associated isotope fractionation would need to be more or less balanced by
635 uptake of Zn into the actual cell, with the preference for light isotopes that is expected for this
636 process, that has been observed in culture, and that has been inferred in lakes. It is noteworthy
637 that Zn attached to the external surfaces of diatoms in culture experiments (John et al., 2007)
638 is either unfractionated with respect to Zn in the medium (low free Zn^{2+} concentrations) or
639 slightly enriched in heavy isotopes (high free Zn^{2+} concentrations). Note that we do not
640 suggest that uptake of Zn into cells does not occur – rather that it may not be the dominant
641 mode of Zn removal from these Southern Ocean surface waters. Indeed, the next section will
642 argue for the regeneration of such an intra-cellular pool to explain the shallow sub-surface

643 data.

644 **6.3 Sub-surface Zn isotopic minima: the signature of regenerated intra-cellular Zn**

645 The clearest and most consistent feature of the Zn isotopic data in the three depth profiles
646 (Fig. 6-8) is seen at the near surface, where data at around 50-70m are distinctly lighter than
647 the datum for the uppermost samples from the same depth profiles. Thus at PS71-163-1, the
648 9m analysis gives δ^{66}Zn = +0.63‰, while the analysis at 40m gives +0.27‰. At PS71-113-2
649 δ^{66}Zn at 10m is +0.80‰ while at 74m it is +0.46‰. At PS71-104-2 δ^{66}Zn = +0.46‰ at 15m
650 and is +0.25‰ at 50m. Thus there is a fairly consistent 0.31±0.09‰ shift to lighter values in
651 the immediate sub-surface from the uppermost level measured. A similar shift is seen at the
652 only other relatively complete depth profile yet published. At the BATS station in the tropical
653 North Atlantic (Boyle et al. 2012), the surface datum is 0.28‰ heavier than that at 75m. Zn
654 isotope data for the upper water column in the NE Pacific (Bermin et al., 2006) show a similar
655 pattern: the datum at 75m is 0.2 per mil lighter than at the surface. At both BATS and the NE
656 Pacific there is then a more gradual move towards a heavier deep ocean value with depth. In
657 the depth profiles presented here this sub-surface minimum in δ^{66}Zn is often quite abrupt,
658 which appears consistent with similarly abrupt changes in physical oceanographic parameters
659 to values that then characterize much of the deeper water column (e.g. Figure 6).

660 Thus, at this early stage, the shift from heavy Zn at the surface to lighter Zn in the immediate
661 sub-surface is developing into a consistent feature of oceanic Zn isotopes. In four out of the
662 five cases outlined above (BATS, NE Pacific, three Southern Ocean profiles), the horizon
663 with the isotopically-light Zn also has higher Zn concentrations than the surface datum.
664 Scavenging of Zn via adsorption onto particulate surfaces preferentially removes the heavy
665 isotope from solution (Maréchal et al., 2000; Pokrovsky et al., 2005; Gélabert et al., 2006;
666 Balistrieri et al., 2008; Juillot et al., 2008) and would thus leave an isotopically-light residual

667 dissolved pool. Though the situation is complicated by the fact that upwelling advects Zn into
668 the upper ocean, the increasing Zn concentrations with depth do not appear to be consistent
669 with scavenging. Moreover, a scavenging origin for the light isotopes at around 50m leaves
670 open the cause, in two of the three depth profiles investigated in the Southern Ocean (PS71-
671 113-2 at +0.8‰ and PS71-163-1 at +0.67‰), of the distinctly heavy isotopic composition of
672 dissolved Zn right at the surface, heavier, for example, than any likely continental source
673 (Little et al., 2013), with nothing to date suggesting that such an input would be heavier than
674 about +0.4‰. Thus, it seems probable that the enrichment of the light isotopes at 50-75m are
675 coupled to a corresponding depletion at the surface. It is most likely then that this isotopic
676 fractionation is driven by a kinetic fractionation (John et al., 2007; Peel et al., 2009)
677 associated with uptake into a cellular pool (surface) and regeneration of that same pool in the
678 very shallow sub-surface.

679 Following the discussion in the sections 6.1 and 6.2, we stress again that uptake of Zn into the
680 cells of phytoplankton for metabolic use is likely to be only one of the processes by which Zn
681 is removed from the surface ocean. In the view presented here, a second process by which Zn
682 is associated with organic material within diatom frustules may often drive the bulk of the Zn
683 depletion in surface water, and we suggest that the lack of correlation between Zn isotopes
684 and Si concentrations (Fig. 10b) implies that this must occur with minimal isotopic
685 fractionation. Thus surface waters in the Southern Ocean do not develop the extremely heavy
686 residual Zn isotopic compositions that would be expected if the observed Zn depletion arose
687 purely from uptake into the interiors of cells with a kinetic isotopic fractionation. The crucial
688 point, however, is that the pool of Zn associated with the opal is regenerated only in the deep
689 ocean, when the opal itself dissolves. Thus, the much shallower regeneration of the light intra-
690 cellular pool shows up as a distinctive feature of the water column at 50-75m, even though the
691 impact of it in the surface ocean is obscured by another process.

692 We acknowledge that this interpretation of the Zn isotopic data is speculative at present, that
693 these qualitative ideas need to be tested experimentally and with further field data, and
694 particularly with at least a one-dimensional numerical model that parameterizes the key
695 processes. Such a model would also have to take account of vertical transport of Zn by
696 advection and diffusion, which would dampen the signature of the biological processes we
697 invoke. Such a one-dimensional model is beyond the scope of the present contribution, but is
698 something that is being actively pursued. As we show in the next section, however, the idea of
699 two broad mechanisms behind the depletion of Zn in surface waters, and different
700 lengthscales for the regeneration of the two resultant pools of Zn in the near surface and deep
701 ocean, also explain some otherwise puzzling features of deep Southern Ocean zinc
702 distributions, and the emerging pattern of Zn isotopes in the deep ocean more generally.

703 **6.4 The Zn isotopic composition of the deep ocean: regeneration of a distinct pool of Zn**

704 As already stated, a striking feature of the Southern Ocean Zn isotope dataset is the
705 homogeneity of the deep ocean. Thus, apart from one outlying datum for the bottom sample at
706 PS71-163 (which may be affected by a sedimentary source), the 17 samples from ≥1000m
707 yield $\delta^{66}Zn = 0.54\pm0.04$ (2 SE). Fig. 11 presents a summary of Zn isotopic composition data
708 from different parts of the world's deep oceans, from this study and from Boyle et al. (2012).
709 The datum plotted on Figure 11 for the deep Pacific is for the SAFE deep sample, one of the
710 intercalibration samples tabulated here (Table 1). Though data are admittedly still scarce, the
711 striking feature of Fig. 11 is the *overall* homogeneity of Zn isotopes in the deep ocean.
712 Beneath 1000m, the $\delta^{66}Zn$ in three geographically widespread locations is essentially
713 identical, with an average and 2sd of +0.53±0.14‰ (2SE = 0.03, n = 21).

714 In common with many oceanographic parameters, it is expected that the greatest variation in
715 Zn isotopic compositions will be found in the upper ocean – it is here that the biogeochemical

716 processes that impart the largest isotopic fractionations are expected to occur. The deep ocean,
717 on the other hand, is where Zn that is cycled between different phases (dissolved, biological
718 and inorganic particulates) in the upper ocean is largely returned to the dissolved phase (e.g.
719 Bruland, 1980). Thus it is perhaps no surprise that the deep ocean is relatively homogeneous.
720 It is more surprising that the deep North Atlantic and the deep North Pacific exhibit no
721 difference in δ^{66}Zn (c.f. δ^{13}C, for example; Kroopnick, 1985) despite the rough factor of 4–5
722 difference in total Zn concentrations between these two water masses.

723 It is very difficult to see how the drawdown of Zn in the surface ocean via cellular uptake
724 with a kinetic isotope fractionation similar to that implied by published culturing and field
725 studies (John et al., 2007; Peel et al., 2009) would not result in a significant isotopic
726 difference between the deep Atlantic and deep Pacific. On the other hand, the homogeneity of
727 deep ocean Zn isotope compositions is perfectly explicable if: (a) intra-cellular Zn is
728 regenerated in the shallow sub-surface as suggested in the previous section; (b) the dominant
729 process by which Zn is removed from the surface ocean is not via such intra-cellular uptake
730 but rather via a process that leads to its ultimate association with the opal frustules of diatoms,
731 one which is not associated with a significant isotopic fractionation; (c) these processes are
732 fast enough that mixing cannot eliminate the isotopic gradients. Such an explanation is, as
733 noted earlier, completely consistent with the similar patterns of Si and Zn regeneration in the
734 deep ocean, while accommodating the two additional observations deriving from culturing
735 studies and the water column data presented here: that Zn in diatoms is predominantly in an
736 organic phase (Ellwood and Hunter, 2000), and that intra-cellular uptake involves a
737 significant isotopic fractionation (John et al., 2007), one that is not consistent with the lack of
738 heavy Zn isotope signatures in the very Zn-depleted surface ocean.

739 **6.5 Zn isotopic composition of the oceans and its relationship to input and output fluxes**
740

741 In terms of the Zn isotopic cycle of the ocean as a whole, the relationship of oceanic dissolved
742 Zn isotope compositions to those of the inputs is clearly important. Thus the second feature
743 illustrated in Fig. 11 is the fact that the average deep ocean dissolved Zn isotopic composition
744 appears to be slightly heavier than the likely continental input (Little et al., 2013). Given the
745 higher Zn concentrations in the deep ocean relative to the surface, and the fact that 75% of the
746 volume of the oceans is also beneath 1000m, the deep ocean value must be very close to the
747 whole ocean average. For example, for the depth profiles in Table 2, as well as for that from
748 the North Atlantic in Boyle et al. (2012), the average of all the data, weighted by
749 concentration, is only 0.04 per mil less than the average of the data beneath 1000m, given
750 earlier as 0.53±0.03 (2SE, n = 21).

751 The input flux to the oceans appears to be dominated by the dissolved riverine flux, with a
752 small but significant source from atmospheric aerosols (Little et al., 2013). A significant
753 hydrothermal input to the oceans has never been identified for Zn in depth profiles measured
754 close to ocean ridges (e.g. Bermin, 2006) in contrast to some other elements (e.g. German et
755 al., 1991 and Middag et al., 2011a for Mn; Klunder et al., 2011 for Fe). It appears that all the
756 (considerable) Zn emanating from hydrothermal systems is very quickly precipitated in
757 sulphides (German et al., 1991) near the source. The hydrothermal fluids that have been
758 measured (John et al., 2008) have a δ^{66}Zn at +0.24‰, slightly lighter than other inputs.

759 Thus an isotopically light sink from the dissolved pool appears to be required by the fact that
760 the dissolved pool is slightly heavier than the inputs. Light sinks from the ocean are well-
761 known for some other transition metals, such as Mo and Cu (e.g. Siebert et al., 2003; Barling
762 and Anbar, 2004; Little et al., 2013) but none of these help with the Zn issue. For example, Zn
763 isotopes in Fe-Mn crusts and nodules are universally heavier than deep seawater (Maréchal et
764 al., 2000; Little et al. 2013), implying not only that this output does not represent the required

765 light sink, but also that if this is a significant output the requirement for a light sink is
766 increased. The single study available of oceanic carbonate (Pichat et al., 2003) suggests that
767 this small sink is also isotopically heavy. The ideas presented in earlier sections suggest that
768 the diatom opal sink of Zn probably closely reflects surface seawater itself and will also be
769 heavier than the inputs (c.f. Andersen et al., 2011), while Zn sorption to organic material
770 should also be either the same as seawater or slightly isotopically heavy (Gélabert et al. 2006;
771 John et al., 2007).

772 The only important removal pathway from the dissolved pool in the oceans that is likely to be
773 isotopically light is the pool of Zn that is taken up intra-cellularly by phytoplankton. As noted
774 in previous sections, a single culturing study (John et al., 2007) has demonstrated that diatoms
775 take up the light isotopes of Zn such that $\Delta_{\text{seawater-diatom cell}}$ = +0.2 to +0.8, with the
776 fractionation varying systematically with the free Zn^{2+} concentration of the medium. A study
777 of a Swiss lake (Peel et al. 2009) has demonstrated that sinking particulates associated with
778 the summer algal bloom have a δ^{66}Zn 0.8‰ lighter than the water column. Moreover,
779 Andersen et al. (2011) invoked the same uptake of light Zn isotopes into phytoplankton
780 organic material to explain the progressively heavier isotopic signature of diatom opal, which
781 these authors interpreted to be recording surface seawater, as upwelled Zn is progressively
782 depleted in the surface waters of the Pacific Sub-Antarctic zone of the Southern Ocean. We
783 have suggested earlier that it is regeneration of this pool that yields the light Zn isotopic
784 composition of the shallow sub-surface in the Southern Ocean and elsewhere.

785 It thus seems likely that the portion of the isotopically light cellular Zn that survives
786 regeneration and is buried in sediments could represent the sink that seems to be required by
787 the oceanic Zn cycle as we understand it thus far. Zn isotopic analysis of organic-rich
788 sediments may provide a means of testing this suggestion. Though fraught with uncertainty, a

789 simple calculation can provide a preliminary assessment of its feasibility. Little et al. (2013)
790 suggest that the magnitude of a missing light sink must be around $3\pm2x10^{8}$ mol yr^{-1},
791 depending on its isotopic composition. Data on the Zn/C ratio of marine phytoplankton are
792 scarce but those in Ho et al. (2003) for a variety of cultured organisms suggest that it is of the
793 order of $0.6x10^{-6}$ mol/mol. Field data for plankton tows in the same paper show Zn/P ratios up
794 to 5 times greater than the cultured organisms. These data would imply a carbon burial rate to
795 achieve the required Zn sink of $0.3\text{-}8x10^{13}$ mol yr^{-1}. Unfortunately large uncertainties on this
796 estimate derive from the input parameters, but the range does span published estimates of
797 carbon burial rates at $1\text{-}2x10^{13}$ mol yr^{-1} (e.g. Hedges and Keil., 1995).

798

799 ## 7. CONCLUDING REMARKS

800 We have reported the first full depth profiles for dissolved Zn isotopes in the ocean, as well as
801 data for a surface transect along the zero meridian in the Atlantic sector of the Southern
802 Ocean. The new isotopic data, taken together with data for the deep North Pacific and
803 published data for the North Atlantic, exhibit three principal features. The first is the
804 homogeneity of the deep ocean, such that the data presented here for beneath 1000m, in
805 combination with more limited data from the North Pacific and North Atlantic, have a $\delta^{66}Zn$ =
806 +0.53±0.14‰ (2SE = 0.03, n = 21). Secondly, and though there are both heavy and light
807 isotopic values in the surface Southern Ocean, there is no systematic shift towards heavy
808 isotopic compositions as would be expected (John et al., 2007; Peel et al., 2009) if the well-
809 established Zn drawdown in the surface ocean is achieved dominantly through intra-cellular
810 uptake of Zn. Thirdly, surface values *are* always heavier than data for the shallow sub-surface
811 (40-80m), both in the dataset presented here and in two published partial depth profiles from
812 the North Atlantic and North Pacific (Bermin et al., 2006; Boyle et al., 2012).

These new Zn isotope data are consistent with a scenario whereby Zn removal from the surface ocean occurs via two processes, a dominant one that does not involve an isotopic fractionation and a lesser one that preferentially removes the light isotope. We suggest that the dominant process is the incorporation of Zn into organic matter associated with diatom frustules, while the second is the metabolic uptake of Zn into the cells of all phytoplankton. Such a hypothesis is consistent with the data presented here, as well as some key observations that have been made about the oceanic Zn cycle in previous work. Firstly, dissolved Zn concentrations in this study and elsewhere are closely tied to Si, but structure in the correlations for surface water (Fig. 10a) suggests a dependence on microbial ecology, in particular the dominance or not of opal-building organisms in the phytoplankton assemblage. The well-established observation of strong Si-Zn concentration correlations is coupled to the fact that there is no systematic relationship at all between Si and Zn isotopes (Fig. 10b), implying that the removal of Zn coupled to Si removal involves little or no isotopic fractionation. On the other hand, increases in Zn concentration with depth down to 80m are associated with distinctly lighter isotopic compositions than the rest of the water column, including the overlying photic zone. We suggest that this is the signature of the regeneration of intra-cellular zinc, while the main increase in Zn concentrations in the deep ocean, closely tied to Si, is the result of the regeneration of organic material intimately associated with diatom frustules, that is only re-mobilised when the opal itself dissolves (c.f. Lohan et al., 2002).

The scenario outlined above is consistent with what we know about the interactions between Zn and its isotopes, Si and biology from experiments and field studies. For example, culture studies have demonstrated that the Zn content in the opal phase of frustules is very small (Ellwood and Hunter, 2000), about 1-3% of the total Zn in diatoms with the rest associated with one or more organic phases. In addition, the Zn/Si ratio of the deep ocean is 1-2 orders of

838 magnitude greater than in diatom opal (e.g. Bruland, 1980; Lohan et al., 2002). Both of these
839 constraints have rendered the close association between Si and Zn concentrations in the deep
840 ocean a real conundrum. A solution to this puzzle is provided by the fact that polysaccharides
841 and proteins coat the silica frustule of diatoms, and that these bear functional groups (e.g.
842 amino, carboxyl) that have a strong affinity for metal ions, including Zn (e.g. Gélabert et al.,
843 2006). Culture experiments have also shown that the Zn associated with these organic
844 substances (Gélabert et al., 2006) is isotopically identical to Zn in the culture medium at free
845 Zn^{2+} concentrations equivalent to those found in the surface ocean (John et al., 2007). In our
846 proposed scenario, it is this Zn that is regenerated with Si, but only when the opal frustule
847 itself dissolves, in the deep ocean. The fact that the uptake of this pool of Zn involves little
848 isotope fractionation explains the lack of a relationship between Si concentrations and Zn
849 isotopes in the portion of the Southern Ocean studied here, where diatoms are an important
850 part of the phytoplankton population. The relative dominance of this process would also
851 explain the fact that the deep Atlantic, the deep Southern Ocean and the deep Pacific are
852 isotopically identical for Zn (Boyle et al., 2012; this study). On the other hand, both culture
853 experiments and field data demonstrate that uptake of Zn into the interiors of cells for
854 metabolic purposes shows the expected preference for the light isotopes (John et al., 2007;
855 Peel et al., 2009). We further suggest, therefore, that this represents a different process, a pool
856 that is regenerated at much shallower levels, and one that explains the light isotopic signature
857 seen at 40-80m in the Southern Ocean, the North Atlantic and the NE Pacific.

858 Clearly these qualitative ideas, though for the first time yielding a wholly consistent picture of
859 the oceanic Zn cycle, need to be tested. They imply, in particular, a decoupling of the shallow
860 and deep ocean for Zn, with the isotopic characteristics of the two being determined by
861 different processes. A quantitative 1D model is required to ascertain, for example, whether the
862 light signal in the shallow sub-surface can be maintained against upward advection of deep

863 waters in the Southern Ocean. A prediction of these ideas would be that the vertical
864 component of the oceanic cycle of Zn and its isotopes would differ in regions where diatoms
865 dominate, as opposed to where non-silica-building organisms are the main contributors to the
866 phytoplankton assemblage.

867 In addition, we have addressed the mass balance of the whole ocean, using the data in this
868 paper, published data for Zn isotopes in other parts of the ocean, and data on the inputs and
869 outputs (Little et al., 2013). The large and homogeneous deep ocean Zn reservoir is about 0.2
870 ‰ heavier than our current best estimate of the inputs of Zn to the ocean, so that an
871 isotopically light sink is required for the whole ocean isotopic mass balance. The sinks that
872 have been characterised, in contrast, are all heavier than the inputs. We advance the working
873 hypothesis that it is the burial of isotopically light Zn in cellular organic matter that represents
874 the light sink from the oceanic dissolved pool. This idea can also be tested through the
875 isotopic analysis of organic-rich sediments.

876

877 **ACKNOWLEDGEMENTS**

878 We gratefully acknowledge the captain, officers and entire crew of the P. S. Polarstern. This
879 work was supported by a UK government Overseas Research Scholarship to YZ and a
880 Leverhulme Research Fellowship to DV. The comments of Associate Editor Mark
881 Rehkämper and those of three anonymous reviewers forced us to think harder about the data
882 and have genuinely turned this into a better paper.

883

884 **REFERENCES**

885 Abouchami W., Galer S.J.G., de Baar H.J.W., Alderkamp A.C., Middag R., Laan P.,
886 Feldmann H. and Andreae M.O. (2011) Modulation of the Southern Ocean cadmium isotope
887 signature by ocean circulation and primary productivity. *Earth Planet. Sci. Lett.* **305**, 83-91.
888 Alderkamp A.C., De Baar H.J.W., Visser R.J.W. and Arrigo K.R. (2010) Can photoinhibition
889 control phytoplankton abundance in deeply mixed water columns of the Southern Ocean?
890 *Limnol. Oceanogr.* **55**, 1248–1264.
891 Altabet M.A. and Francois R. (1994) Sedimentary nitrogen isotopic ratio records surface
892 ocean NO_3 – utilization. *Global. Biogeochem. Cyc.* **8**, 103-116.
893 Andersen M.B., Vance D., Archer C., Anderson R.F., Ellwood M.J. and Allen C.S. (2011)
894 The Zn abundance and isotopic composition of diatom frustules, a proxy for Zn availability in
895 ocean surface seawater. *Earth Planet. Sci. Lett.* **301**, 137-145.
896 Archer C. and Vance D. (2004) Mass discrimination correction in multiple-collector plasma
897 source mass spectrometry: an example using Cu and Zn isotopes. *J. Anal. At. Spectrom*. **19**,
898 656-665.
899 Balistrieri L.S., Borrok D.M., Wanty R.B. and Ridley W.I. (2008) Fractionation of Cu and Zn
900 isotopes during adsorption onto amorphous Fe(III) oxyhydroxide: experimental mixing of
901 acid rock drainage and ambient river water. *Geochim. Cosmochim. Acta* **72**, 311-328.
902 Barling J. and Anbar A.D. (2004) Molybdenum isotope fractionation during adsorption by
903 manganese oxides. *Earth Planet. Sci. Lett.* **217**, 315-329.
904 Bermin J., Vance D., Archer C. and Statham P.J. (2006) The determination of the isotopic
905 composition of Cu and Zn in seawater. *Chem. Geol.* **226**, 280-297.
906 Bermin J. (2006) *Determination of the isotopic composition of Cu and Zn in seawater.* PhD
907 dissertation, Royal Holloway, University of London.

908 Boyd P.W. and Elwood M.J. (2010) The biogeochemical cycle of iron in the ocean. *Nat.*
909 *Geosci.* **3**, 675-682.
910 Boyd P.W and 35 others (2000) A mesoscale phytoplankton bloom in the polar Southern
911 Ocean stimulated by iron fertilization. *Nature* **407**, 695-702.
912 Boyle E.A. and 20 others (2012) Geotraces IC1 (BATS) contamination-prone trace element
913 isotopes Cd, Fe, Pb, Zn, Cu and Mo intercalibration. *Limnol. Oceanogr. – Methods* **10**, 653-
914 665.
915 Brand L.E., Sunda W.G. and Guillard R.R.L. (1983) Limitation of marine phytoplankton
916 reproductive rates by zinc, manganese and iron. *Limnol. Oceanogr.* **28**, 1182-1198.
917 Bruland K.W. (1980) Oceanographic distributions of cadmium, zinc, nickel, and copper in the
918 North Pacific. *Earth Planet. Sci. Lett.* **47**(2), 176-198.
919 Bruland K.W. (1989) Complexation of zinc by natural organic ligands in the Central North
920 Pacific. *Limnol. Oceanogr.* **34**(2), 269-285.
921 Bruland K.W., Lohan M.C. (2003) Controls of Trace Metals in Seawater. In *Treatise on*
922 *Geochemistry*, vol. 6 (ed H. Elderfield). Elsevier, Amsterdam, pp. 23-47.
923 Buitenhuis E.T., Timmermans K.R. and de Baar H. (2003) Zinc-bicarbonate colimitation of
924 Emiliania huxleyi. *Limnol. Oceanogr.* **48**(4), 1575-1582.
925 Buma A.G.J., de Baar H.J.W., Nolting R.F. and van Bennekom A.J. (1991) Metal enrichment
926 experiments in the Weddell-Scotia Seas: effects of Fe and Mn on various plankton
927 communities. *Limnol. Oceanogr.* **36**, 1865-1878.
928 Cloquet C., Carignan J. and Libourel, G. (2006) Isotopic composition of Zn and Pb
929 atmospheric depositions in an urban/periurban area of northeastern France. *Env. Sci. Tech.* **40**,
930 6594-6600.
931 Coale K.H., Gordon R.M. and Wang X. (2005) The distribution and behavior of the dissolved
932 and particulate iron and zinc in the Ross Sea and Antarctic Circumpolar Current along 70^{o} W.

Deep-Sea Res. **52**, 295-318.

Crawford D.W., Lipsen M.S., Purdie D.A., Lohan M.C., Statham P.J., Whitney F.A., Putland J.N., Johnson W.K., Sutherland N., Peterson T.D., Harrison P.J. and Wong C.S. (2003) Influence of zinc and iron enrichments on phytoplankton growth in the northeastern subarctic Pacific. *Limnol. Oceanogr.* **48**, 1583-1600.

Croot P.L., Baars O. and Streu P. (2011) The distribution of dissolved zinc in the Atlantic sector of the Southern Ocean. *Deep-Sea Res. II.* **58**, 2707-2719.

Cullen J.T. (1991) Hypotheses to explain high nutrient conditions in the open sea. *Limnol. Oceanogr.* **36**, 1579-1599.

de Baar H.J.W., Buma A.G.J., Nolting R.F., Cadée G.C., Jacques G. and Tréguer P.J. (1990) On iron limitation of the Southern Ocean: experimental observations in the Weddell and Scotia Seas. *Mar. Ecol. Prog. Ser.* **65**, 105-122.

de Baar H., de Jong J.T.M., Bakker D.C.E., Löscher B.M., Veth C., Bathmann U. and Smetacek V. (1995) Importance of iron for plankton blooms and carbon dioxide drawdown in the Southern Ocean. *Nature* **373**, 412-415.

de Baar H.J.W. and 33 others (2005) Synthesis of iron fertilization experiments: from the Iron Age in the Age of Enlightenment. *J. Geophys. Res.* **110**, C09S16, doi: 10.1029/2004JC002601.

de Baar H., Timmermans K.R., Laan P., de Porto H.H., Ober S., Blom J.J., Bakker M.C., Schilling J., Sarthou G., Smit M.G. and Klunder M. (2008) Titan: a new facility for ultraclean sampling of trace elements and isotopes in the deep oceans in the international Geotraces program. *Mar. Chem.* **111**, 4-21.

De La Rocha C.L., Brzezinski M.A., DeNiro M.J. and Shemesh A. (1998) Silicon-isotope composition of diatoms as an indicator of past oceanic change. *Nature* **395**, 680-683.

Donat J.R., Bruland K.W. (1990) A comparison of two voltammetric techniques for

958 determining zinc speciation in northeast Pacific Ocean waters. *Mar. Chem.* **28**, 301-323.
959 Ellwood M.J. and Hunter, K. (2000) The incorporation of zinc and iron into the frustule of the
960 marine diatom *Thalassiosira pseudonana*. *Limnol. Oceanogr.* **45**, 1517-1524.
961 Ellwood M.J. and van den Berg C.M.G. (2000) Zinc speciation in the Northeastern Atlantic
962 Ocean. *Mar. Chem.* **68**, 295-306.
963 Fahrbach E. and de Baar H. (2010) The Expedition of the Research Vessel "Polarstern" to the
964 Antarctic in 2008 (ANT-XXIV/3). *Reports on Polar and Marine Research*
965 hdl:10013/epic.34050.
966 Gélabert A., Pokrovsky O.S., Viers J., Schott J., Boudou A and Feurtet-Mazel A. (2006)
967 Interaction between zinc and freshwater and marine diatom species: Surface complexation
968 and Zn isotope fractionation. *Geochim. Cosmochim. Acta* **70**, 839-857.
969 German C.R., Fleer A.P., Bacon M.P. and Edmond J.M. (1991) Hydrothermal scavenging at
970 the Mid Atlantic Ridge: Radionuclide distributions. *Earth Planet. Sci. Lett.* **107**, 101-114.
971 Grasshoff K., Fleming K. and Ehrhardt M. (1999) *Methods of Seawater Analysis*. Verlag
972 Wiley-VCH, Weinheim, 632pp.
973 Hassler C.S., Sinoir M., Clementson L.A. and Butler E.C.V. (2012) Exploring the link
974 between micro-nutrients and phytoplankton in the Southern Ocean during the 2007 austral
975 summer. *Front Microbiol*. **3**, 202.
976 Hedges J.I. and Keil R.G. (1995) Sedimentary organic matter preservation: an assessment and
977 speculative synthesis. *Mar. Chem.* **49**, 81-115.
978 Ho T.-Y., Quigg A., Finkel Z.V., Milligan A.J., Wyman K., Falkowski P.G. and Morel
979 F.M.M. (2003) The elemental composition of some marine phytoplankton. *J. Phycol.* **39**,
980 1145-1159.
981 John S.G, Geis R.W., Saito M.A. and Boyle E.A. (2007) Zinc isotope fractionation during
982 high-affinity and low-affinity zinc transport by the marine diatom *Thalassiosira oceanica.*

983 *Limnol. Oceanogr.* **52**, 2710-2714.

984 John S.G., Rouxel O.J., Craddock P.R., Engwall A.M. and Boyle E.A. (2008) Zinc stable
985 isotopes in seafloor hydrothermal vent fluids and chimneys. *Earth Planet. Sci. Lett.* **269**, 17-
986 28.

987 Juillot F., Marechal C., Ponthieu M., Cacaly S., Morin G., Benedetti M., Hazemann J.L.,
988 Proux O. and Guyot F. (2008) Zn isotopic fractionation caused by sorption on goethite and 2-
989 Lines ferrihydrite. *Geochim. Cosmochim. Acta* **72**, 4886-4900.

990 Kingston H.M., Barnes I.L., Brady T.J. and Rains T.C. (1978) Separation of eight transition
991 elements from alkali and alkaline earth elements in estuarine and seawater with chelating
992 resin and their determination by graphite furnace atomic absorption spectrometry. *Anal.*
993 *Chem.* **50**, 2065-2070.

994 Klunder M.B., Laan P., Middag R., de Baar H.J.W. and van Oiijen J.C. (2011) Dissolved iron
995 in the Southern Ocean (Atlantic sector). *Deep-Sea Res. II* **58**, 2678-2694.

996 Kroopnick P.M. (1985) The distribution of ^{13}C of ΣCO_2 in the world oceans. *Deep-Sea Res. I.*
997 **32**, 57-84.

998 Lippard S.J. and Berg J.M. (1994) *Principles of Bioinorganic Chemistry*. University Science
999 books, Mill Valley, CA, USA.

1000 Little S.H., Vance D., Walker-Brown C. and Landing W.M. (2013) The oceanic mass balance
1001 of Cu and Zn isotopes, investigated by analysis of their inputs and oxic output in
1002 ferromanganese crusts. *Geochim. Cosmochim. Acta*, submitted.

1003 Lohan M.C., Statham P.J. and Crawford D.W. (2002) Total dissolved zinc in the upper water
1004 column of the subarctic North East Pacific. *Deep-Sea Res. II* **49**, 5793-5808.

1005 Löscher B.M. (1999) Relationships among Ni, Cu, Zn and major nutrients in the Southern
1006 Ocean. *Mar. Chem.* **6**, 67-102.

1007 Maréchal C.N., Télouk P. and Albarède F. (1999) Precise analysis of copper and zinc isotopic
1008 compositions by plasma-source mass spectrometry. *Chem. Geol.* **156**, 251-273.
1009 Maréchal C.N., Nicolas E., Douchet C. and Albarède F. (2000) Abundance of zinc isotopes as
1010 a marine biogeochemical tracer. *Geochem. Geophys. Geosyst.* **1**, 1999GC000029.
1011 Marinov I., Gnanadesikan A., Toggweiler J.R. and Sarmiento J.L. (2006) The Southern Ocean
1012 biogeochemical divide. *Nature* **441**, 964-967.
1013 Martin J.H., Gordon R.M., Fitzwater S. and Broenkow W.W. (1989) VERTEX:
1014 phytoplankton/iron studies in the Gulf of Alaska. *Deep-Sea Res.* **36**, 649-680.
1015 Martin J.H., Fitzwater S.E and Gordon R.M. (1990) Iron deficiency limits phytoplankton
1016 growth in Antarctic Waters. *Global. Biogeochem. Cyc.* **4**, 5-12.
1017 Middag R., de Baar H.J.W., Laan P., Cai P.H. and van Ooijen J. (2011a) Dissolved
1018 manganese in the Atlantic sector of the Southern Ocean. *Deep-Sea Res. II* **58**, 2661–2677
1019 Middag R., van Slooten C., de Baar H.J.W. and Laan P. (2011b) Dissolved aluminium in the
1020 Southern Ocean. *Deep-Sea Res. II* **58**, 2647-2660.
1021 Minas H.J., Minas M. and Packard T.T. (1986) Productivity in upwelling areas deduced from
1022 hydrographic and chemical fields. *Limnol. Oceanogr.* **31**, 1182-1206.
1023 Mitchell B.G., Brody E.A., Holm-Hansen O., McClain C. and Bishop J. (1991) Light
1024 limitation of phytoplankton biomass and macronutrient utilization in the Southern Ocean.
1025 *Limnol. Oceanogr.* **36**, 1662-1677.
1026 Morel F.M.M., Reinfelder J.R., Chamberlain C.P., Roberts S.B., Lee J.G. and Yee D. (1994)
1027 Zinc and carbon co-limitation of marine phytoplankton. *Nature* **369**, 740-742.
1028 Orsi A.H., Whitworth III T. and Nowlin W.D. (1995) On the meridional extent and fronts of
1029 the Antarctic Circumpolar Current. *Deep-Sea Res.* **42**, 641-673.
1030 Peel K., Weiss D. and Sigg L. (2009) Zinc isotope composition of settling particles as a proxy
1031 for biogeochemical processes in lakes: insights from the eutrophic Lake Greifen, Switzerland.

1032 *Limnol. Oceanogr.* **54**, 1699-1708.

1033 Pichat S., Douchet C. and Albarede F. (2003) Zinc isotope variations in deep-sea carbonates
1034 from the eastern equatorial Pacific over the last 175 ka. *Earth Planet. Sci. Lett.* **210**, 167-178.

1035 Pokrovsky O.S., Viers J. and Freydier R. (2005) Zinc stable isotope fractionation during its
1036 adsorption on oxides and hydroxides. *J. Colloid. Interf. Sci.* **291**, 192-200.

1037 Queguiner B., Treguer P., Peeken I. and Scharek R. (1997) Biogeochemical dynamics and the
1038 silicon cycle in the Atlantic sector of the Southern Ocean during austral spring 1992. *Deep-*
1039 *Sea Res. II* **44**, 69-89.

1040 Scharek R., van Leeuwe M.A. and de Baar H.J.W. (1997) Responses of Southern Ocean
1041 phytoplankton to addition of trace metals. *Deep-Sea Res. II*, **44**, 209-227

1042 Schlitzer R. (2002) Ocean Data View, http://www.awi-bremerhaven.de/GEO/ODV.

1043 Shaked Y., Xu Y., Leblanc K. and Morel F.M.M. (2006) Zinc availability and alkaline
1044 phosphatase activity in *Emiliania huxleyi*: Implications for Zn-P co-limitation in the ocean.
1045 *Limnol. Oceanogr.* **51**, 299-309.

1046 Siebert C., Nägler T., von Blanckenburg F. and Kramers J.D. (2003) Molybdenum isotope
1047 records as a potential new proxy for paleoceanography. *Earth Planet. Sci. Lett.* **211**, 159-171.

1048 Sinoir M., Butler E.C.V., Bowie A.R., Mongin M., Nesterenko P.N., and Hassler C.S. (2012)
1049 Zinc marine biogeochemistry in seawater: a review. *Mar. Freshwater. Res.* **63**, 644-657.

1050 Sunda W.G. and Huntsman S.A. (1992) Feedback interactions between zinc and
1051 phytoplankton in seawater. *Limnol. Oceanogr.* **37**, 25-40.

1052 Sunda W.G. and Huntsman S.A. (1995) Cobalt and zinc inter-replacement in marine
1053 phytoplankton: biological and geochemical implications. *Limnol. Oceanogr.* **40**, 1404-1407.

1054 Sunda W.G. and Huntsman S.A. (1997) Interrelated influence of iron, light and cell size on
1055 marine phytoplankton growth. *Nature* **390**, 389-392.

1056 Sunda W.G. and Huntsman S.A. (2005) Effect of CO_2 supply and demand on zinc uptake and
1057 growth limitation in a coastal diatom. *Limnol. Oceanogr.* **50**, 1181-1192.
1058 Weiss D.J., Mason T.F.D., Zhao F.J., Kirk G.J.D., Coles B.J. and Horstwood M.S.A. (2005)
1059 Isotopic discrimination of zinc in higher plants. *New. Phytol.* **165**, 703-710.
1060 Wu J. and Boyle E.A. (1998) Determination of iron in seawater by high-resolution isotope
1061 dilution inductively coupled plasma mass spectrometry after $Mg(OH)_2$ coprecipitation. *Anal.*
1062 *Chim. Acta* **367**, 183-191.
1063

1064 **Table 1:** Zn isotopic and concentration analyses of intercalibration samples obtained from the
1065 Bruland laboratory at Santa Cruz.

Sample ID	Depth (m)	[Zn] (nmol/kg)	δ^{66}Zn (‰)	2 sigma	Total Zn from ID (ng)	Yield (%)
SAFe D2[a]	1000	7.66	0.52	0.03	103	91
SAFe D1	1000	7.68	0.56	0.03	85	91
SAFe D2	1000	7.40	0.52	0.03	76	96
SAFe D2	1000	7.38	0.50	0.04	74	95
SAFe S[b]	Surface	0.051			17	85
SAFe S	Surface	0.052			17	91
SAFe S	Surface	0.050			17	59
SAFe S	Surface	0.049			16	60
GSC32[c]	Surface	1.35	0.08	0.04	48	99
GSC303[c]	Surface	1.37	0.18	0.06	47	97

1066
1067 [a] SAFe deep samples (central North Pacific) obtained from Geoffrey Smith (University of California, Santa
1068 Cruz). Each line on the table is for a separate analysis from two different bottles (D1 or D2).
1069 [b] SAFe surface samples (central North Pacific) obtained from Geoffrey Smith (University of California, Santa
1070 Cruz). Each line is for a separate analysis from four different 4 litre bottles. These analyses were done at a stage
1071 when we had not developed the methodology fully for small samples and isotopic data were not obtained.
1072 [c] Samples from the Santa Barbara Basin (eastern North Pacific) obtained from Geoffrey Smith (University of
1073 California, Santa Cruz). Each line is a separate analysis of different 1 litre bottles.
1074

1075 **Table 2**: Zn concentration (nmol/kg) and δ^{66}Zn for three vertical profiles in the Atlantic sector
1076 of the Southern Ocean.

IPY ID	Depth (m)	[Zn] (nmol/kg)	δ^{66}Zn (‰)	2 sigma[1]	Total Zn[2] in analysis (ng)	Yield (%)	[Si][3] (µmol/kg)
Station PS71-104-2 (47°39.36'S, 4°15.7'E)							
PS71-104-2-24	15	0.32	0.47	0.07	51	72	1.86
PS71-104-2-22	50	0.62	0.25	0.05	86	80	1.86
PS71-104-2-20	101	0.71	0.43	0.05	103	77	5.66
PS71-104-2-18	202	1.03	0.41	0.04	129	74	10.2
PS71-104-2-16	301	2.10	0.47	0.04	68	95	20.4
PS71-104-2-14	399	2.45	0.44	0.05	79	99	28.1
PS71-104-2-11	998	5.35	0.44	0.06	79	99	65.1
PS71-104-2-9	1500	5.33	0.43	0.05	78	105	68.7
PS71-104-2-8	1748	4.88	0.48	0.05	53	98	70.7
PS71-104-2-7	1997	4.88	0.50	0.07	49	101	72.0
PS71-104-2-6	2499	5.83	0.51	0.05	54	97	89.1
PS71-104-2-5	3002	6.16	0.60	0.06	56	96	101
PS71-104-2-3	4006	8.04	0.61	0.05	83	99	118
PS71-104-2-2	4202	7.03	0.54	0.06	70	92	119
Station PS71-113-2 (52°59.828'S, 0.2°0.05'W)							
PS71-113-2-24	10	3.06	0.80	0.06	83	92	35.4
PS71-113-2-22	74	2.59	0.47	0.03	72	111	35.6
PS71-113-2-19	101	2.69	0.54	0.04	76	108	35.8
PS71-113-2-14	298	6.25	0.39	0.03	68	95	83.5
PS71-113-2-12	401	6.56	0.48	0.04	51	93	87.8
PS71-113-2-10	500	6.27	0.40	0.04	51	95	90.8
PS71-113-2-7	1000	6.30	0.70	0.05	49	95	103
PS71-113-2-5	1501	7.07	0.58	0.04	55	92	115
PS71-113-2-3	1997	6.82	0.50	0.03	52	93	123
PS71-113-2-1	2351	6.84	0.43	0.06	49	93	128
Station PS71-163-1 (67°S, 0°E)							
PS71-163-1-24	9	2.57	0.67	0.04	34	94	62.6
PS71-163-1-22	45	4.42	0.27	0.05	203	86	64.8
PS71-163-1-20	74	7.03	0.53	0.03	99	89	89.8
PS71-163-1-18	171	7.08	0.49	0.03	98	85	95.6
PS71-163-1-16	250	7.18	0.44	0.03	99	86	98.6
PS71-163-1-14	401	7.14	0.57	0.03	98	92	104
PS71-163-1-13	748	7.56	0.53	0.03	99	91	113
PS71-163-1-11	1001	7.73	0.64	0.03	91	88	118
PS71-163-1-9	1501	7.79	0.55	0.03	90	90	123
PS71-163-1-7	2000	7.62	0.59	0.03	104	78	124
PS71-163-1-5	3000	7.60	0.55	0.02	104	86	123
PS71-163-1-3	4002	7.30	0.53	0.02	98	86	124
PS71-163-1-1	4601	7.35	0.96	0.04	78	92	129

1077 [1] Internal uncertainty, with all measurement uncertainties propagated through the double spike reduction
1078 procedure. Long-term standard reproducibility is greater at 0.08‰ (see text).
1079 [2] Total Zn analyses as obtained from the isotope dilution analysis. Total procedural blanks were 2-3 ng and the
1080 reported concentrations (in nmol/kg) are corrected for this blank.
1081 [2] Si data here and in Table 3 from Middag et al. (2011a).

Table 3: Zn concentration (nmol/kg) and δ^{66}Zn for 11 surface (2-5m depth) transect stations in the Atlantic sector of the Southern Ocean.

IPY ID	Longitude (°E)	Latitude (°S)	[Zn] (nmol/kg)	δ^{66}Zn (‰)	2 sigma[1]	Total Zn[2] (ng)	Yield (%)	[Si] (µmol/kg)
PS71-105	3.82	48.04	0.63	0.14	0.06	88	75	1.89
PS71-105	3.82	48.04	0.65	0.07	0.04	42	99	
PS71-105	3.82	48.04	0.65	0.11	0.03	41	98	
PS71-109	0.00	51.67	1.27	0.60	0.04	85	90	15.7
PS71-111[3]	-0.54	52.17	6.44	0.48	0.05	219	93	23.3
PS71-111	-0.54	52.17	6.55	0.46	0.04	86	101	
PS71-111	-0.54	52.17	6.53	0.42	0.03	106	97	
PS71-111	-0.54	52.17	6.32	0.49	0.03	82	90	
PS71-111	-0.54	52.17	6.55	0.45	0.04	88	89	
PS71-114	0.00	53.18	2.69	0.45	0.04	90	95	34.3
PS71-117	0.02	54.32	2.76	0.58	0.04	96	92	44.3
PS71-120	0.00	55.24	2.81	0.58	0.03	95	98	50.3
PS71-123	0.00	56.30	3.25	0.50	0.03	88	106	63.8
PS71-126	0.00	57.21	3.47	0.51	0.04	96	93	64.8
PS71-129	0.00	58.20	3.69	0.50	0.04	102	96	67.1
PS71-133	0.00	59.00	3.02	0.45	0.03	84	102	62.7
PS71-136	0.00	60.24	2.72	0.52	0.04	76	105	62.1
PS71-139	0.00	61.15	2.26	0.50	0.04	62	101	57.6

[1] Internal uncertainty, with all measurement uncertainties propagated through the double spike reduction procedure. Long-term standard reproducibility is greater at 0.08‰ (see text).

[2] Total Zn analyses as obtained from the isotope dilution analysis. Total procedural blanks were 2-3 ng and the reported concentrations (in nmol/kg) are corrected for this blank.

[3] Zn concentrations for sample PS111 reproduce across duplicate analyses of separate aliquots from the same 20 litre MPI container, but the data are highly anomalous. We suspect that the original 20 litre MPI bottle must have been contaminated before or during original sampling, and these data are not considered further.

Figure Captions

Fig. 1: A portion of the IPY ANT-XXIV/3 cruise track with sampling stations, positions of the Antarctic fronts and oceanographic regimes (see Orsi et al., 1995). AAZ = Antarctic Zone, PFZ = Polar Frontal Zone, SAZ = Subantarctic Zone, WG = Weddell Gyre, ACC = Antarctic Circumpolar Current, STF = Subtropical Front, SAF = Subantarctic Front, APF = Antarctic Polar Front, SB-ACC = Southern Boundary of ACC. Grey arrows and associated labels show schematic surface flow directions. The Bristol lab received 3 depth profiles (see red boxes) and a subset of large surface samples (all surface samples collected are indicated by filled black circles). Asterisks mark stations sampled with ultraclean Titan frame (de Baar et al., 2008), which includes all three depth profiles analysed here for Zn.

Fig. 2: N-S vertical section for dissolved silicate (μmol/kg) along the Greenwich Zero Meridian. The line at the top shows the major fronts (green) and oceanic regimes (black) discussed in the text. Abbreviations are as in Figure 1. The depth profiles studied for Zn isotopes and concentrations are marked in white. Silicate data plotted using the ODV software (Schlitzer, 2002).

Fig. 3: Isotopic data for pre-co-precipitated seawater supernatant samples and MQ samples to which Zn JMC standard has been added. “Seawater 30 ng”, “Seawater 200 ng” represent the supernatant samples to which 30 ng and 200 ng standard Zn were added respectively. The result obtained for the supernatant samples was $\delta^{66}Zn = +0.08 \pm 0.03‰$ (n=12). The slightly elevated $\delta^{66}Zn$ suggests that a small amount of Zn was left in these samples after co-precipitation. The result for MQ samples was $\delta^{66}Zn = -0.01 \pm 0.02‰$ (n=8), all falling within the error of the expected 0‰, demonstrating the robustness of the double spike approach.

Fig. 4: Plot of measured Zn isotopic data for 4L surface Equatorial Atlantic samples to which various amounts of JMC standard and double spike have been added, versus the reciprocal Zn

amounts. In this case the original sample Zn was not removed, previous isotope dilution analysis having indicated that sample Zn concentrations were very small, at 0.01-0.04 nmol kg^{-1}.

Fig. 5: Plot of measured Zn concentration data for Station PS71-113-2 (red squares) compared with data for the same location in Croot et al. (2011) (green triangles) and with data for a composite of nearby stations (895, 897, 947, 949) published in Löscher (1999). The latter data are plotted as blue diamonds, with obvious outliers in this older dataset highlighted by the open symbols. Beneath 1000m the data obtained here are in very good agreement with Löscher (1999) while the data of Croot et al. (2011) are displaced towards lower values.

Fig. 6: Depth profiles of potential temperature (°C), salinity, oxygen concentration (µmol/kg), silicon (µmol/kg), dissolved Zn concentration (nmol/kg), Zn isotopic composition (‰) of samples collected at station **PS71-163-1 (67°S, 0°E)**. Salinities are reported on the Practical Salinity Scale (PSS78). Water mass abbreviations: AASW = Antarctic Surface Water; CIW = Central Intermediate Water; WSDW = Weddell Sea Deep Water; WSBW = Weddell Sea Bottom Water.

Fig. 7: Depth profiles of potential temperature (°C), salinity, oxygen concentration (µmol/kg), silicon (µmol/kg), dissolved Zn concentration (nmol/kg), Zn isotopic composition (‰) of samples collected at station **PS71-113-2 (52°59.828'S, 0.2°0.05'W)**. Water mass abbreviations as in Figure 6 plus: AAIW = Antarctic Intermediate Water; UCDW = Upper Circumpolar Deep Water; LCDW = Lower Circumpolar Deep Water; WSBW = Weddell Sea Bottom Water.

Fig. 8: Depth profiles of potential temperature (°C), salinity, oxygen concentration (µmol/kg), silicon (µmol/kg), dissolved Zn concentration (nmol/kg), Zn isotopic composition (‰) of

1143 samples collected at station **PS71-104-2 (47°39.36'S, 4°15.7'E)**. Water mass abbreviations as
1144 in Figure 6,7 plus: NADW = North Atlantic Deep Water.

1145 **Fig. 9:** Plots of measured salinity, Si concentration (µmol/kg), dissolved Zn concentration
1146 (nmol/kg), Zn isotopic composition δ^{66}Zn (‰) of surface transect samples (filled diamonds)
1147 and near surface samples (open diamonds) collected at vertical profiles PS71-104-2, PS71-
1148 113-2, PS71-163-1 against latitude. Abbreviations for surface oceanographic regimes as in
1149 Fig. 1.

1150 **Fig. 10:** Cross-plots of Si concentrations versus (a) the new Zn concentration and (b) isotopic
1151 data. Data from the ACC (north of 56°S) are plotted as red squares and data from the Weddell
1152 Gyre (WG, south of 56°S) as blue circles. Solid symbols are for surface samples (collected at
1153 2-5m and presented in Table 3), and open symbols for sub-surface (from depths ≥ 10m, as
1154 presented in Table 2) and deep samples.

1155 **Fig. 11**: A summary of Zn isotopic data thus far available for different parts of the world's
1156 deep oceans (≤1000m), compared to estimates of the likely inputs to the ocean (Little et al.,
1157 2013). The solid vertical line shows the δ^{66}Zn of rivers, the dashed line that for Atlantic
1158 aerosols, and the dot-dash line that for silicate rocks and sediments of the continental crust (all
1159 compiled in Little et al., 2013). Blue filled diamonds represent the deep North Atlantic
1160 (BATS; Boyle et al. 2012), red filled squares the deep North Pacific (SAFe; this study), and
1161 green filled triangles the deep Southern Ocean (Atlantic sector, this study, arranged by depth
1162 (green arrow), and omitting the bottom-most sample from Station PS71-163). Data plotted for
1163 Southern Ocean samples are single analyses and their associated analytical uncertainties
1164 (±0.08‰). Data for the Atlantic and Pacific are averages and 2SEs of multiple analyses of the
1165 same sample. The shaded green band shows 2SE either side of the mean for all the deep ocean
1166 data.

1167 **Zhao et al. – Figure 1**

1168

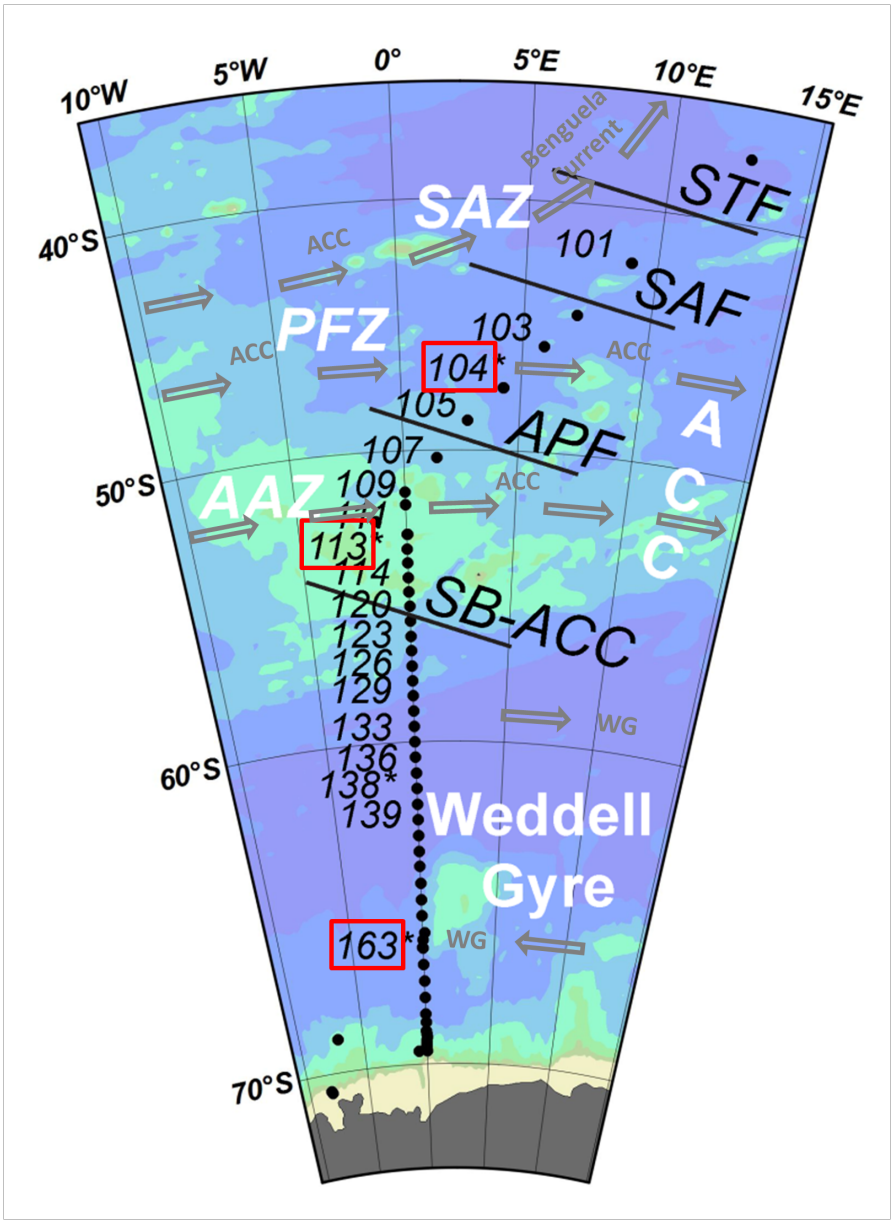

1169

1170

1171

1172 **Zhao et al. – Figure 2**

1173

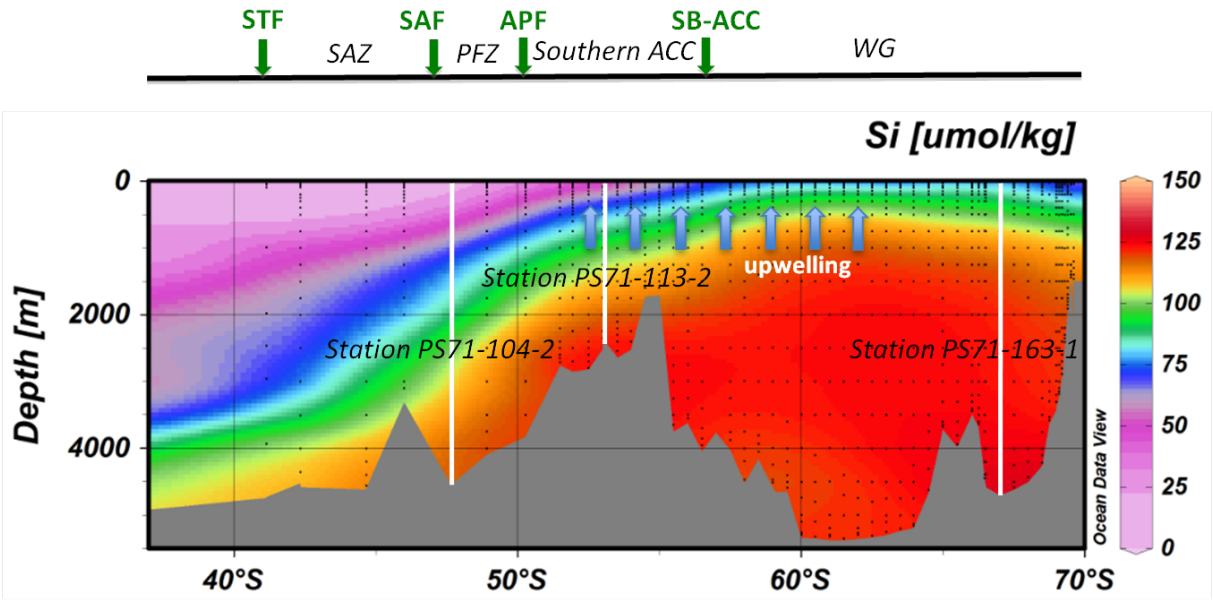

1174

1175

1176 **Zhao et al. – Figure 3**

1177

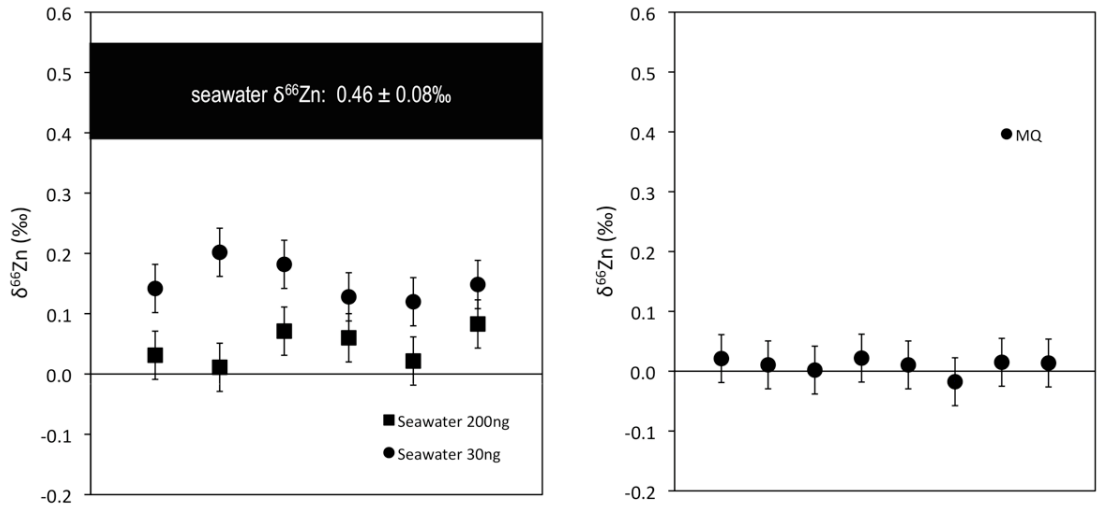

1178

1179

1180 **Zhao et al. – Figure 4**

1181

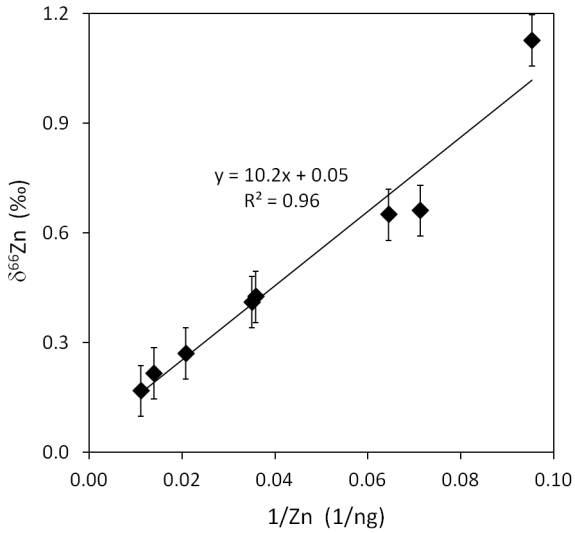

1182

1183

1184

1185 **Zhao et al. – Figure 5**

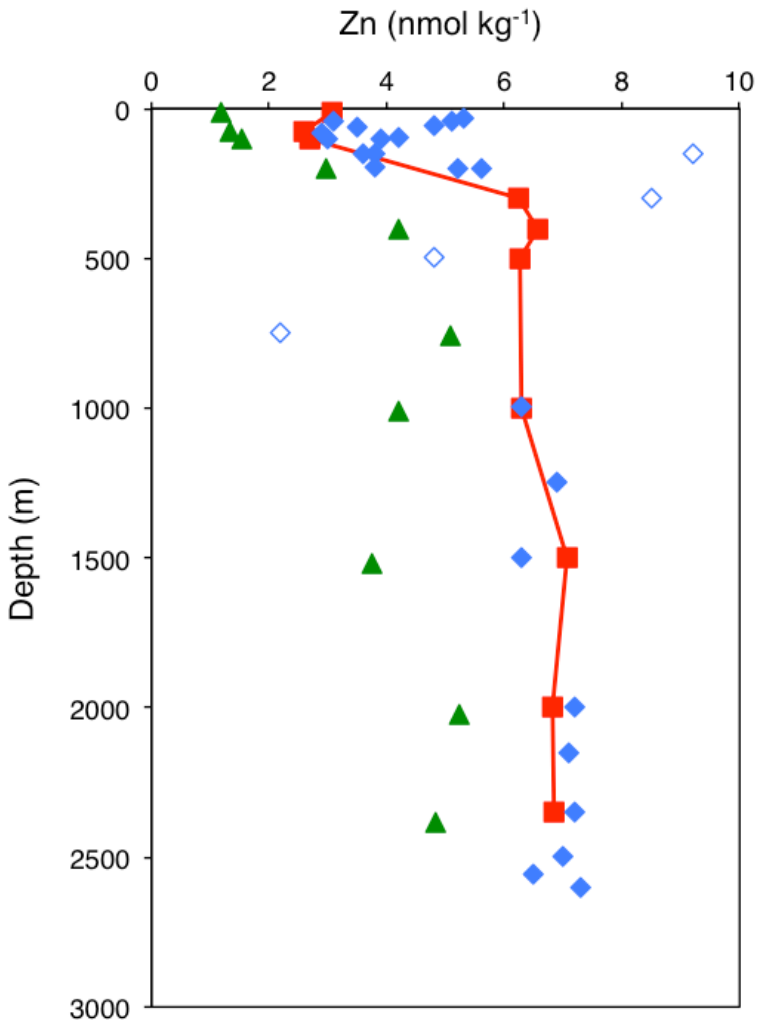

1186

Zhao et al. – Figure 6

PS71-163-1

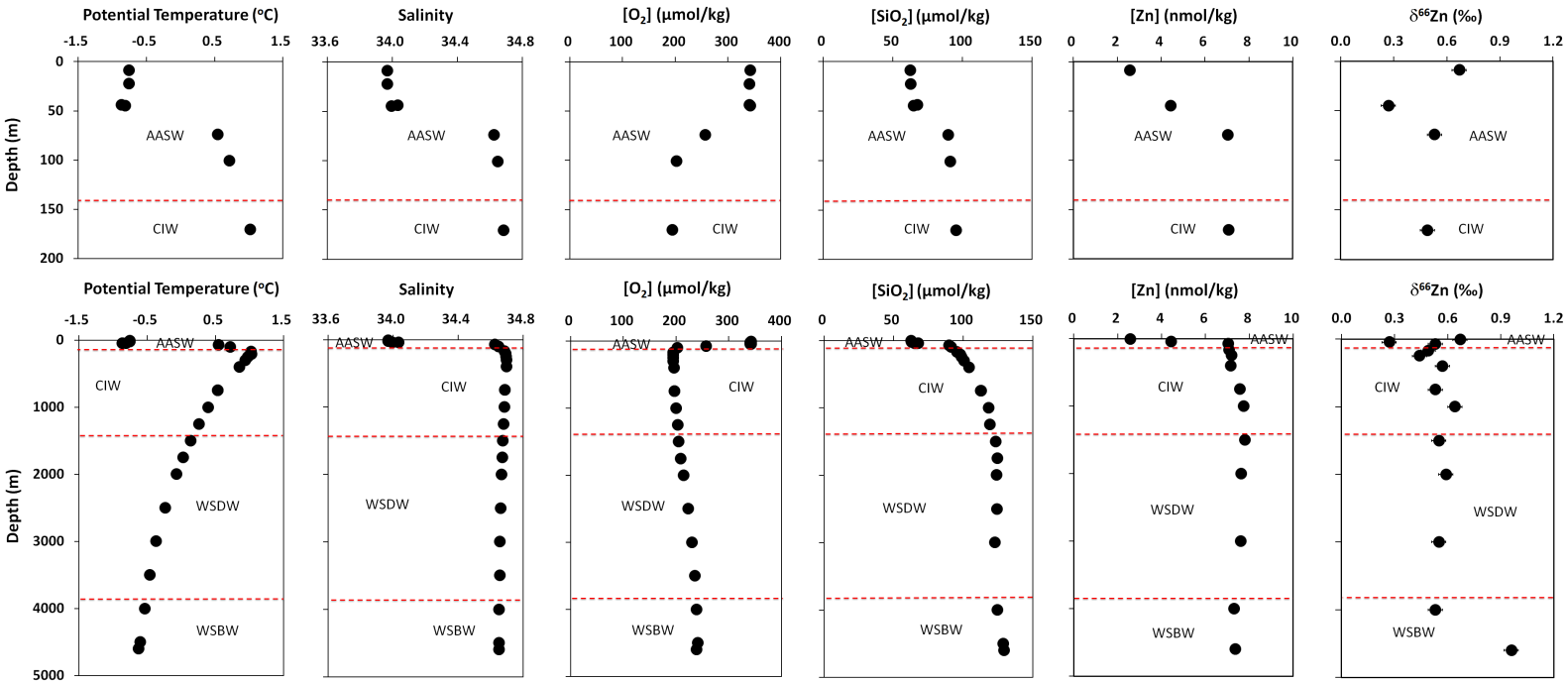

Zhao et al. – Figure 7

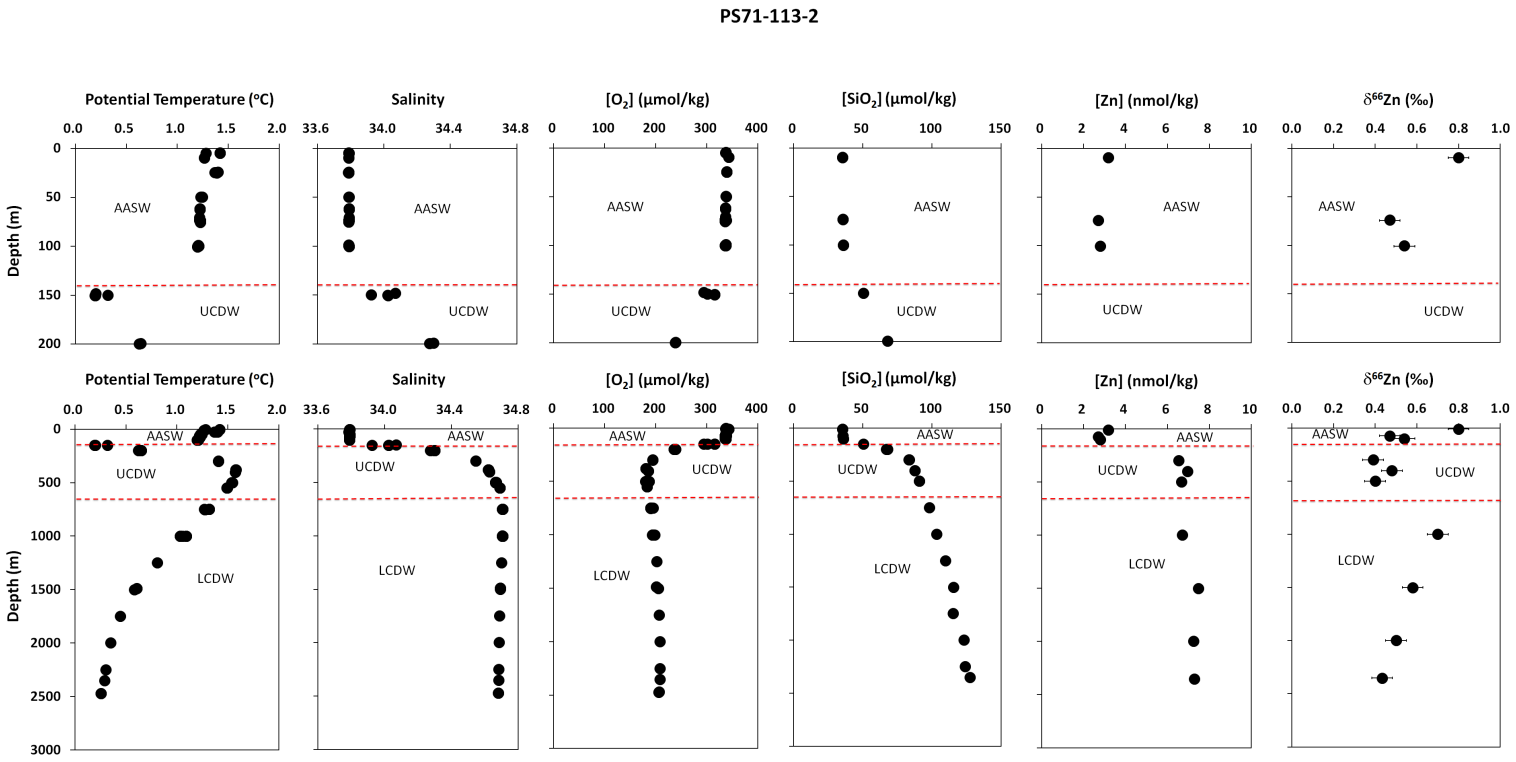

Zhao et al. – Figure 8

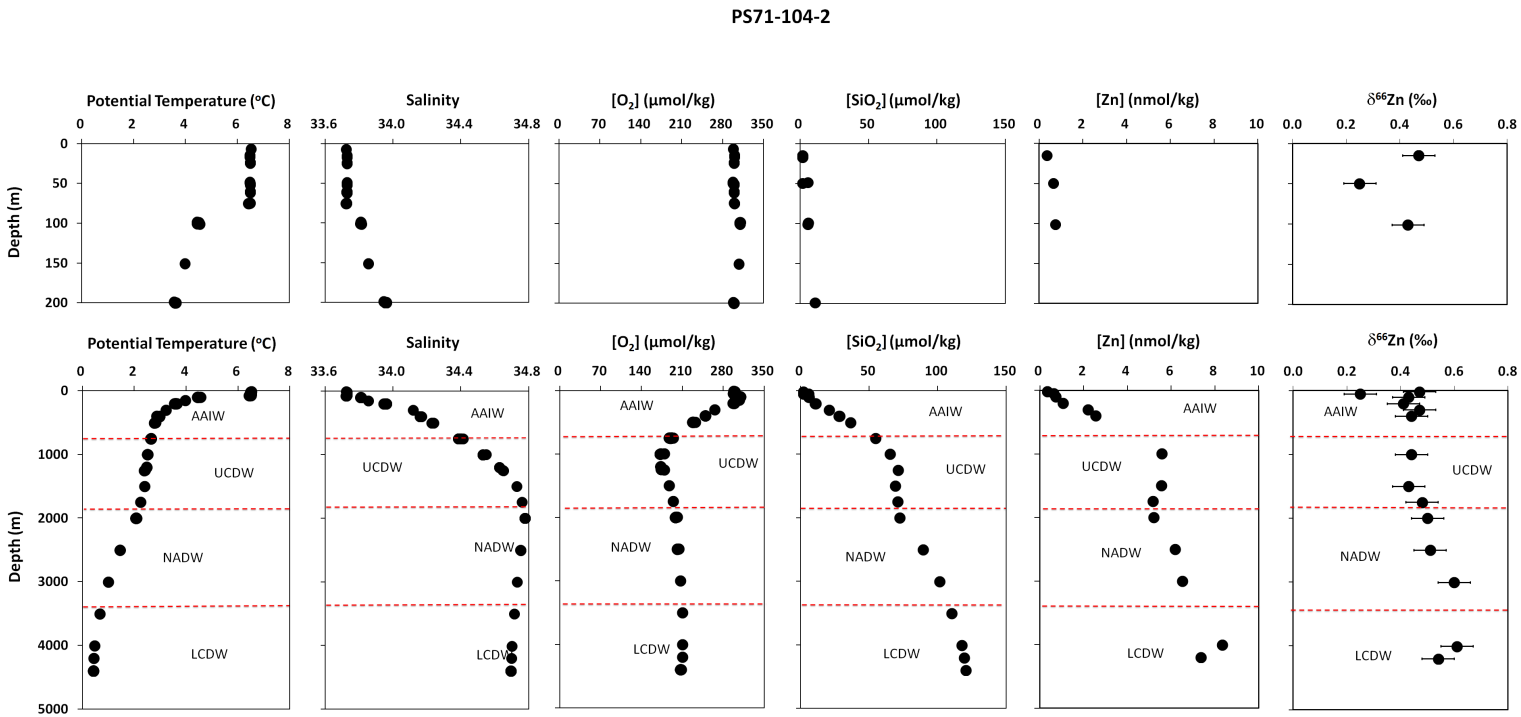

1195

Zhao et al. – Figure 9

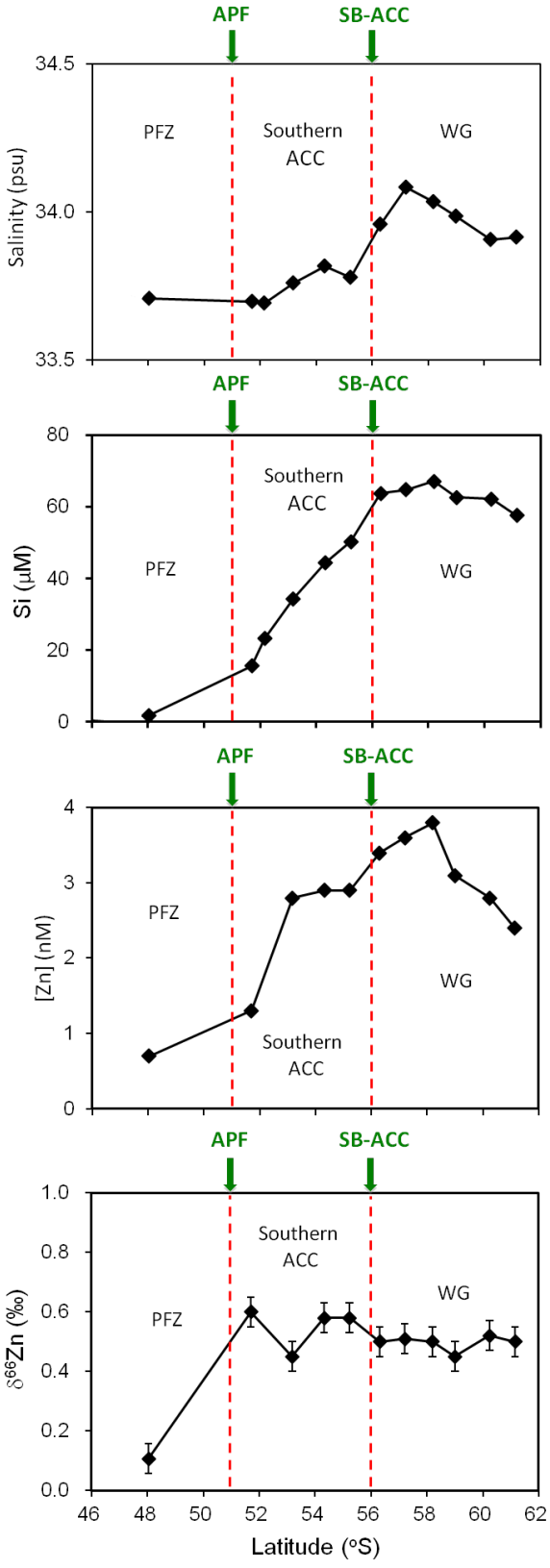

1196

1197

1198 **Zhao et al. – Figure 10**

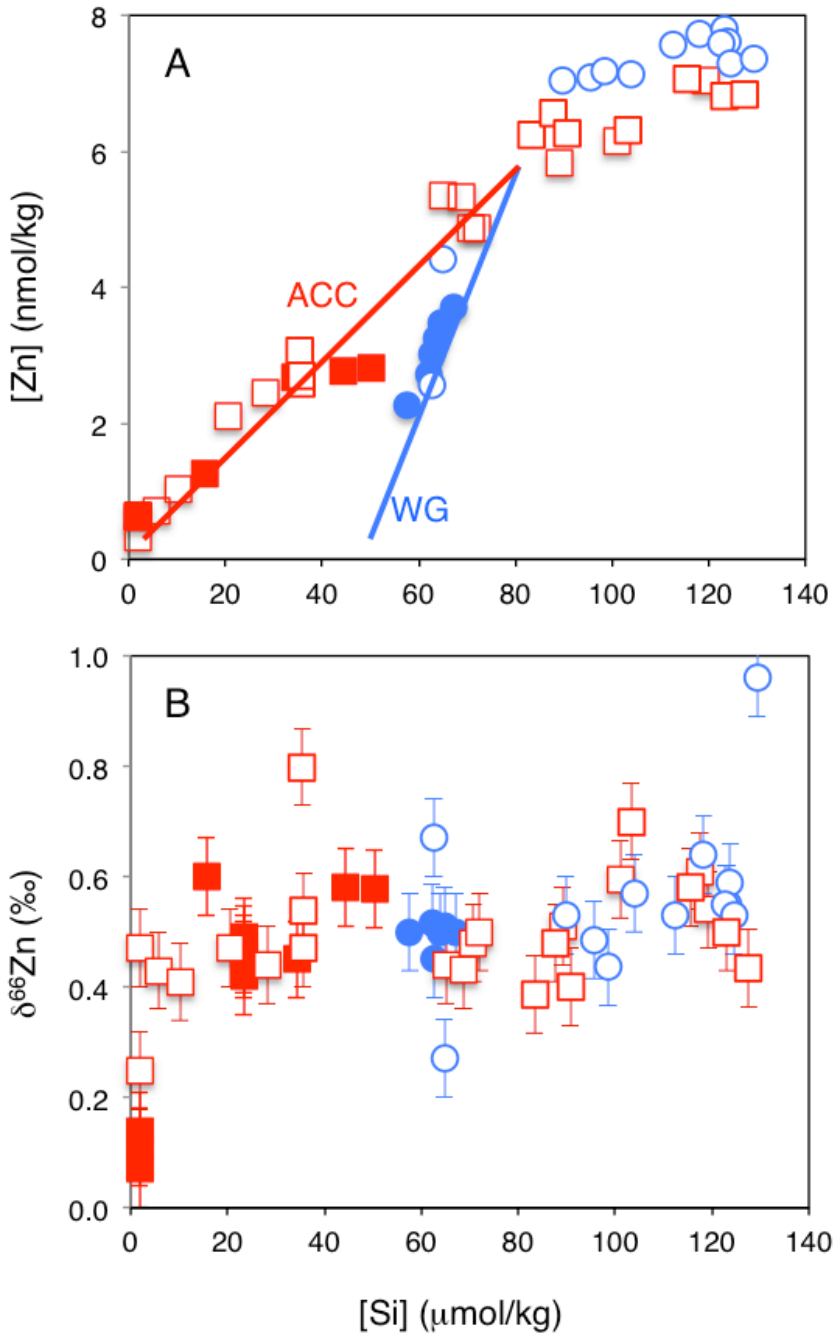

1199

1200

1201 **Zhao et al. – Figure 11**

1202

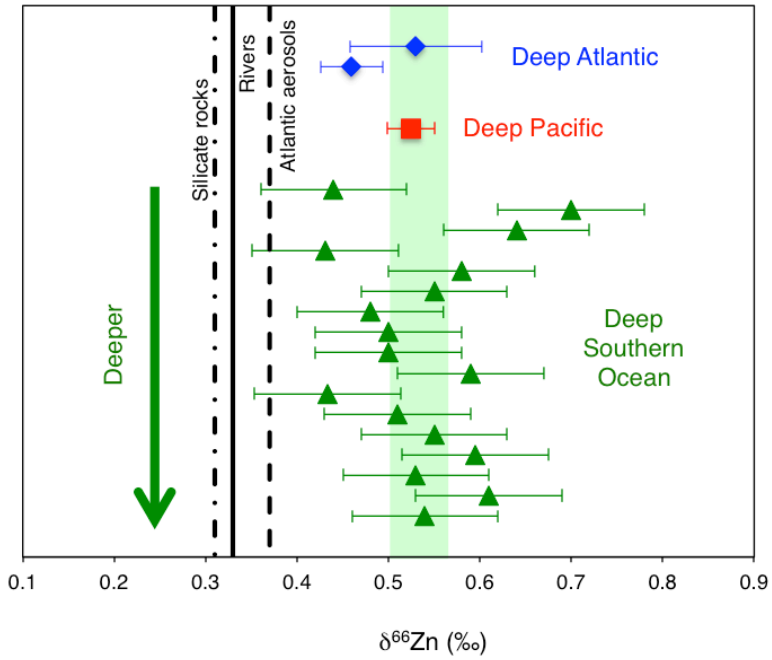

1203

1204

1205

1206